

---

# MAXIMIZING THE PSYCHO-ACOUSTIC SWEET SPOT

---

PREPRINT

 **Pedro Izquierdo Lehmann**

Institute for Mathematical and Computational Engineering  
Pontificia Universidad Católica de Chile  
pizquierdo2@uc.cl

 **Rodrigo F. Cádiz**

Department of Electrical Engineering and  
Music Institute  
Pontificia Universidad Católica de Chile  
rcadiz@uc.cl

 **Carlos A. Sing Long\***

Institute for Mathematical and Computational Engineering and  
Institute for Biological and Medical Engineering  
Pontificia Universidad Católica de Chile  
casinglo@uc.cl

January 6, 2022

**ABSTRACT**

In this work, we let the *sweet spot* be the region where a sound wave generated by an array of loudspeakers is psycho-acoustically close to a desired auditory scene, and we develop a method that aims to generate a sound wave that directly maximizes this sweet spot. Our method incorporates psycho-acoustic principles from the onset and is flexible: while it imposes little to no constraints on the regions of interest, the arrangement of loudspeakers or their radiation pattern, it allows for a wide array of psycho-acoustic models that include state-of-the-art monaural psycho-acoustic models. Our method leverages tools from analysis and optimization that allow for its mathematical analysis and efficient implementation. Our numerical results show that our method yields larger sweet spots compared to some state-of-the-art methods when performing sound field reconstruction for sinusoidal signals using van de Par's psycho-acoustic model.

**Keywords** Spatial sound · sound field reconstruction · psychoacoustics · sweet spot · applied functional analysis · non-convex optimization · DC optimization

**1 Introduction**

The field of spatial sound addresses the question: *how do we create a desired auditory scene over a spatial region of interest from a sound scene generated with only a few loudspeakers?* In this context, the *sound scene* represents the objective nature of a sound wave propagating in the physical world, whereas the *auditory scene* represents the imprint of the sound scene in our subjectivity, that is, the result of the auditory system perceiving and organizing sound into meaning [1, 2]. Over the last century, several methods have been proposed to answer this question. Their performance can be compared in terms of the size of the region where the sound scene creates an auditory scene that most closely resembles the desired one. In this work, we call this region the *sweet spot*.

A popular strategy to recreate an auditory scene is to directly approximate the sound wave that created it. In the literature, this strategy is called *sound field reconstruction* and, in this context, the sweet spot is assumed to be the same as the region where the generated sound wave closely resembles the target sound wave. Following Huygens' principle, any sound scene can be approximated accurately with a sufficiently dense arrangement of loudspeakers. However,

---

\*C. A. Sing Long is also with ANID – Millennium Science Initiative Program – Millennium Nucleus Center for the Discovery of Structures in Complex Data, and with ANID – Millennium Science Initiative Program – Millennium Nucleus Center for Cardiovascular Magnetic Resonance.

---

selecting the audio signals for the loudspeakers is an *ill-conditioned* problem [3] for which there might be multiple solutions, rendering the problem *ill-posed* [4]. Three classes of commonly used methods for sound field reconstruction are *mode matching methods*, *pressure matching methods* and *wave field synthesis*.

Mode Matching Methods (MMM) find an approximation by matching the coefficients in the expansion of the target and generated sound waves in spatial spherical harmonics [5]. Some well-known MMMs are Ambisonics [6], Higher-Order Ambisonics (HOA), and Near-Field Compensated Ambisonics (NFC-HOA) [7]. All of them minimize the  $\ell^2$ -norm of the difference between leading coefficients. Ambisonics assumes the loudspeakers emit plane waves and uses only the leading coefficient, whereas HOA uses a larger but fixed number of coefficients. In contrast, NFC-HOA assumes the loudspeakers are monopoles. Ambisonics, HOA and NFC-HOA are designed for circular or spherical regions of interest. When approximating a plane wave, they create a spherical sweet spot with a radius that is inversely proportional to the frequency of the source [8].

Instead of using expansions in spatial spherical harmonics, Pressure Matching Methods (PMM) minimize the spatio-temporal  $L^2$ -error between the target and generated sound waves [9]. The magnitude of the audio signals are often penalized by their  $L^p$ -norm to mitigate the effects of ill-conditioning [10]. Typically the loudspeakers are modeled as monopoles. In most cases, the solution can only be found numerically, and the discretization of the region of interest plays an important role.

Finally, Wave Field Synthesis (WFS) leverages the single-layer boundary integral representation of a sound wave over a region of interest [11]. Traditional WFS [12] uses a Rayleigh integral representation to derive a solution when the speakers are modeled as dipoles lying on a line. This was later extended to monopoles [13]. Its reformulation, Revisited WFS [14], uses a Kirchhoff-Helmholtz integral representation along with a Neumann boundary condition to obtain a solution for an arbitrary distribution of monopoles. It has been shown that the spatial properties of the auditory scene are correctly simulated by WFS and do not depend on the position of the listener over the region of interest [15]. However, it suffers from coloration effects due to spatial aliasing artifacts [16].

There is extensive literature analyzing these methods and comparing their performance [7, 17, 18]. In fact, they become equivalent in the limit of a continuum of loudspeakers, differing only when using a finite number [19]. Although they are amenable to mathematical analysis and have computationally efficient implementations, their construction has no natural psycho-acoustic justification to produce a large sweet spot as we have defined it. As a consequence, the artifacts introduced by these methods, due to approximation errors, may produce noticeable, and possibly avoidable, psycho-acoustic artifacts.

An alternative to reproduce better the auditory scene is to explicitly account for psycho-acoustic principles [20, 2] in the methods. The first steps in this direction were taken in [21] by proposing a simple model that aims to preserve the spatial properties of the desired auditory scene. A method to reproduce an active intensity field, itself a proxy for the spatial properties, that is largely uniform in space was then proposed in [22]. It is based on an optimization problem yielding audio signals where at most two loudspeakers are active simultaneously. However, it makes the restrictive assumption that the target sound wave is a plane wave, and that the loudspeakers emit plane waves. In [23] the *radiation method* and the *precedence fade* are proposed. The former is equivalent to applying a PMM over a selection of frequencies that are most relevant psycho-acoustically, whereas the latter is a method to overcome the localization problems associated to the *precedence effect* [2]. Finally, in [24] a PMM is extended to account for psycho-acoustic effects by considering the  $L^2$ -norm of the differences in pressure convolved in time by a suitable filter.

We believe that there is a gap between methods that aim to directly approximate a sound wave to reproduce a desired auditory scene, and methods that leverage psycho-acoustic models to reproduce the same auditory scene. In this work, we develop a method that incorporates monaural psycho-acoustic models to generate a sound wave that directly maximizes the sweet spot. This method is amenable to mathematical analysis, has an efficient computational implementation, and incorporates psycho-acoustic principles from the onset. Our numerical results show our method outperforms some state-of-the-art methods for sound field reconstruction. The paper is organized as follows. In Section 2 we introduce the main physical and psycho-acoustic models that we use. In Section 3 we formulate the problem of maximizing the sweet spot, proposing an accurate approximation, and analyzing its properties. In Section 4 we show this approximation can be recast as Difference-of-Convex (DC) program, and we introduce the SWEET algorithm as an efficient method to solve it approximately. In Section 5 we show a concrete implementation of our method based on van de Par’s spectral psycho-acoustic model [25]. Finally, in Section 6 we perform several numerical experiments analyzing its performance, comparing its results with WFS, NFC-HOA and PMM, and showing some concrete applications.

## 2 Mathematical model

### 2.1 Acoustic framework

Consider an array of  $n_s$  speakers located at  $x_1, \dots, x_{n_s} \in \mathbb{R}^3$ . When the medium is assumed homogeneous and isotropic, and each loudspeaker is modeled as an isotropic point source, the sound wave they generate is [26, Section 2.5.2]

$$u(t, x) = \sum_{k=1}^{n_s} \frac{c_k(t - c_s^{-1}\|x - x_k\|)}{4\pi\|x - x_k\|}$$

where  $c_s$  is the speed of sound in the medium, and  $c_1, \dots, c_{n_s}$  are the audio signals of every loudspeaker. In the frequency domain, this is represented as

$$\hat{u}(f, x) = \sum_{k=1}^{n_s} \hat{c}_k(f) \frac{e^{-2\pi i c_s^{-1} f \|x - x_k\|}}{4\pi\|x - x_k\|} \quad (1)$$

where  $\hat{c}_k$  is the Fourier transform of  $c_k$  in time

$$\hat{c}_k(f) := \int c_k(t) e^{-2\pi i f t} dt.$$

To model the spatial radiation pattern of each loudspeaker, along with time-invariant effects such as reverb [27, 28], the representation (1) can be replaced by

$$\hat{u}(f, x) = \sum_{k=1}^{n_s} \hat{c}_k(f) G_k(f, x). \quad (2)$$

where  $G_k$  are the corresponding Green's functions. In addition to this array, consider a bounded domain  $\Omega \subset \mathbb{R}^3$  containing no loudspeakers, i.e.  $x_k \notin \bar{\Omega}$ , allowing us to avoid the singularities in (1) at each  $x_k$ . On this domain, we could attempt to approximate *as best as possible* a sound wave  $u_0$  with the array of loudspeakers.

If we had a continuum of isotropic point sources on  $\partial\Omega$  then, under suitable conditions, the *simple source formulation* [29, Section 8.7] shows we can reproduce  $u_0$  *exactly*. However, when only a finite number of physical loudspeakers are available, we must find  $\hat{c}_1, \dots, \hat{c}_{n_s}$  such that

$$\hat{u}_0(f, x) \approx \sum_{k=1}^{n_s} \hat{c}_k(f) G_k(f, x), \quad (3)$$

in an suitable sense, for  $x \in \Omega$ . In many cases  $\hat{u}_0$  is real-analytic on its second argument over  $\Omega$ . As a consequence, when the speakers are isotropic point sources or  $G_k$  is real-analytic on its 2nd argument, the approximation cannot be exact on *any* open set unless  $u_0$  was actually generated by the speaker array [30, Corollary 1.2.5]. This suggests (3) can hold only in average.

From now on we let  $W_S$  be the set of acoustic waves that can be generated by the array, represented in the frequency domain as in (2). We formalize this set in Section 3 and we first turn our attention to the psycho-acoustic criteria that determine a suitable sense to interpret (3).

### 2.2 Psycho-acoustic preliminaries

To interpret (3) adequately, we consider two basic aspects of the human auditory system: the hearing threshold and the damage/discomfort risk level threshold. The former allows us to determine when the differences between  $u_0$  and the approximating wave are negligible, whereas the latter ensures we do not harm listeners.

#### 2.2.1 The hearing threshold

An important psycho-acoustic problem is to determine when the difference between two audio signals  $v_0 = v_0(t)$  and  $v = v(t)$  is audible. A key concept to address it is the *absolute threshold of hearing* [20, Section 2.1] (see Figure 1): when  $v_0 \equiv 0$ , a pure tone  $v$  is imperceptible if its intensity falls below it.

In complex audio signals other mechanisms come into play and the criteria for perception depend on the signal  $v_0$  being approximated. It has been proposed that the human auditory system first computes an *internal representation* of the audio signal  $v \mapsto \Phi(v)$  to then apply an *internal detector*  $(\Phi(v), \Phi(v_0)) \mapsto D^*(\Phi(v), \Phi(v_0))$ . The difference

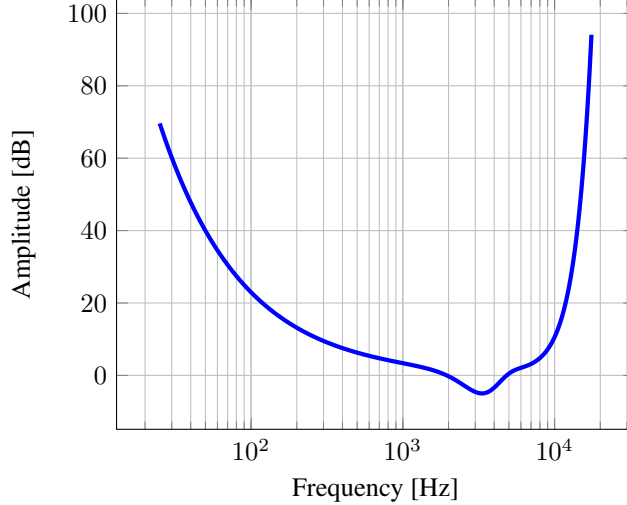


Figure 1: Threshold of audibility.

is perceptible if this value exceeds a given threshold [31, 32]. These studies do not provide a tractable form for this representation nor for the internal detector. A simplification yielding a tractable model is given in [33]. The model is simplified to a non-symmetric *distortion measure*

$$D(v, v_0) = \int_{\mathbb{R}} |L(v - v_0)(t)|^2 dt \quad (4)$$

where  $L$  is a transform modelling locally time-invariant filters that may depend on  $v_0$ . Another simplification in the literature is to consider a sum of convolved-weighted-squared errors [34]

$$D(v, v_0) = \sum_k \int_{\mathbb{R}} |h_k * (v - v_0)(t)g_k(t)|^2 dt \quad (5)$$

where  $h_k$  and  $g_k$  represent a spectral and time weighting respectively. Together they model the difference over the  $k$ -th *auditory filter*. The filters may depend themselves on  $v_0$ . A further simplification introduced in [25] consists in taking a constant  $g$ , i.e.,

$$D(v, v_0) = \sum_k \int_{\mathbb{R}} |\hat{v}(f) - \hat{v}_0(f)|^2 \rho_k(f) df. \quad (6)$$

This proposal works only with spectral information and thus it may not capture temporal *masking* effects accurately [34]. The main reason to make these models dependent on  $v_0$  is to account for the psycho-acoustic equivalence of  $v$  and  $v_0$  when the approximation error is masked by  $v_0$ . This is a principle already used in audio coding [35, 36].

### 2.2.2 The damage and discomfort risk threshold

Exposure to loud sound waves may be uncomfortable. Then, unrestricted spatial sound systems may reproduce undesirable sound scenes where some features prevail at the expense of the discomfort of some listeners. Empirical thresholds for loud discomforts levels for sinusoidal signals over a finite set of frequencies have been defined in the literature, e.g. in [37, 38]. Naturally, these can be expressed as

$$\int |\hat{u}(f, x)|^2 \rho(f)^2 df, \quad (7)$$

where  $\rho(f)$  is the multiplicative inverse of the threshold.

### 2.3 Psycho-acoustic framework

Although there is no definitive model for the hearing threshold, the literature supports the idea that the effects that must be taken into account depend on the sound wave  $u_0$  itself. In this work we consider a general form for these models that includes some proposals in the literature. Inspired by (4), if  $u$  is a acoustic wave on  $\Omega$ , a map of the form

$$Bu(x) = \int \left| \int K_B(t, t', x)(u - u_0)(t', x) dt' \right|^2 dt \quad (8)$$

where  $K_B$  is a suitable kernel, not necessarily time-invariant, quantifies the differences in perception between  $u$  and  $u_0$  at a given  $x$ . A map of this form can account for time-variant effects, such as temporal masking, and also for time-invariant effects, such as spectral masking. Therefore, by choosing suitable kernels we can represent the differences in perception over several auditory filters as a collection of functionals  $B_1, \dots, B_{n_b}$  of the form (8). Consequently, we define the *threshold map* as

$$Tu(x) := \Psi(B_1 u(x), \dots, B_{n_b} u(x)) \quad (9)$$

where  $\Psi : \mathbb{R}_+^{n_b} \rightarrow \mathbb{R}$  is a continuous convex function that is non-decreasing on each one of its components. Without loss, we consider the difference between  $u$  and  $u_0$  is *not audible* at  $x$  if  $Tu(x) \leq 0$ . Remark that by choosing a suitable function  $\Psi$  we may incorporate interactions between different auditory filters. Note that the form (9) encompasses (4), (5) and (6).

Therefore, given an approximating wave  $u \in W_S$ , we define its *sweet spot* as the set where  $u$  is psycho-acoustically equivalent to  $u_0$ , i.e.,

$$\mathcal{S}(u) = \{x \in \Omega : Tu(x) \leq 0\}. \quad (10)$$

Note the psycho-acoustic equivalence that defines the sweet spot is *monaural*. Although at each point the audio signal is in this sense equivalent to the original, this does not account *a priori* for *binaural* effects, e.g., whether the position of an audio source is perceived correctly.

Analogously, to model the discomfort level threshold we consider a collection of functionals  $Q_1, \dots, Q_{n_p}$  of the form (8) with  $u_0 \equiv 0$ . Note that those generalize (7) as they can account for time-variant effects. To enhance flexibility, we do not assume the same selection of auditory filters for the functionals  $B$  and  $Q$ , nor that  $n_b = n_p$ . Hence, we define the *discomfort map*  $P$  as in (9) for  $u_0 \equiv 0$

$$Pu(x) := \Pi(Q_1 u(x), \dots, Q_{n_p} u(x))$$

where  $\Pi$  is a function with the same properties as  $\Psi$ . Then,

$$\mathcal{P} := \{u : \forall x \in \Omega. Pu(x) \leq 0\} \quad (11)$$

is the collection of sound waves below the discomfort threshold at every  $x$ . The domain of  $T$  and  $P$  are sound waves, and thus are part of the *sound scene*. In contrast, their image are part of the *auditory scene*. Hence,  $T$  and  $P$  link the objective and subjective aspects of the problem.

Our goal is to find an acoustic wave  $u \in W_S$  that maximizes the *weighted area* of the sweet spot  $\mu(\mathcal{S}(u))$  while remaining comfortable, i.e.,  $u \in \mathcal{P}$ . From now on, we assume  $u_0$  is known and fixed. Particularly, all the parameters that we have introduced to define the threshold map (9) may depend on  $u_0$ .

### 3 Maximizing the sweet-spot

To formalize the problem of maximizing the sweet spot we make some critical assumptions. We consider the space

$$W := \left\{ u : \sup_{x \in \Omega} \int |u(t, x)|^2 dt < \infty \right\}$$

of sound waves that have finite energy at every  $x \in \Omega$ . Spaces of this form are called *mixed  $L^p$ -spaces* and were introduced in [39]. The space  $W$  is complete under the norm

$$\|u\|_W := \sup_{x \in \Omega} \left( \int |u(t, x)|^2 dt \right)^{1/2}.$$

An important feature of this norm is that the energy is preserved in time and frequency, i.e.,  $\|u\|_W = \|\widehat{u}\|_W$ . From now on, we assume  $u_0 \in W$ . The following proposition summarizes the technical results that ensure that the methods we propose are well-posed. We defer its proof to Appendix A.

**Proposition 1.** *Suppose that*

- (i) *The audio signals  $\widehat{c}_k$  in (2) are all bandlimited to an interval  $I_c$  and their  $L^2$ -norm is uniformly bounded.*
- (ii) *The functions  $G_k$  in (2) are continuous and bounded on  $I_c \times \overline{\Omega}$ .*
- (iii) *For every  $K \in \{K_{B_1}, \dots, K_{B_{n_b}}\} \cup \{K_{Q_1}, \dots, K_{Q_{n_p}}\}$  there is a constant  $C_K$  such that*

$$\int |K(t, t', x)| dt, \int |K(t, t', x)| dt' \leq C_K$$

*for a.e.  $x \in \Omega$ .*

Then the following assertions are true.

- (i) The map  $T : W \rightarrow L^\infty(\Omega)$  is continuous, and for almost every  $x \in \Omega$  the map  $u \rightarrow Tu(x)$  is convex.
- (ii) The set  $\mathcal{S}(u)$  is Borel measurable for any  $u \in W$ .
- (iii) The set  $W_S$  is compact in  $W$ .
- (iv) The set  $\mathcal{P}$  is closed in  $W$ .

We assume the hypotheses of the proposition hold throughout. This does not impose strong constraints on the threshold map (9). However, this implies the sound waves in  $W_S$  are continuous in space and time.

The weighted area of the sweet spot is measured with a Borel measure  $\mu$  [40, Section 1.2]. The problem of maximizing the sweet spot becomes

$$(P_0) \quad \begin{cases} \text{maximize} & \mu(\mathcal{S}(u)) \\ & u \in W_S \\ \text{subject to} & u \in \mathcal{P}. \end{cases}$$

In the above problem the feasible set is closed and bounded and, in fact, compact. To prove there exists a solution, we need to characterize the regularity of the objective function. However, this implies characterizing the behavior of the *set-valued function*  $u \mapsto \mathcal{S}(u)$ . This could be very difficult in practice. For this reason, we propose an approximation to  $(P_0)$  that can be analyzed with standard methods, and for which approximate solutions can be found efficiently.

### 3.1 The layer-cake representation

The *layer-cake representation* allows us to approximate the area of  $\mathcal{S}(u)$  in terms of an integral over a function of  $u$ . Let  $\varphi$  be a bounded non-negative function of bounded variation such that  $\varphi(t) = 0$  for  $t < 0$  and  $\|\varphi\|_{L^1} = 1$ . Let  $\varphi_\varepsilon$  denote the function  $\varphi_\varepsilon(t) = (1/\varepsilon)\varphi(t/\varepsilon)$  for  $\varepsilon > 0$  and define

$$\Phi_\varepsilon(t) = \int_{-\infty}^t \varphi_\varepsilon(s) ds.$$

Suppose  $v \in L^\infty(\Omega)$ ,  $\alpha > 0$  and let  $S_\alpha := \{x : v(x) > \alpha\}$ . Since  $\Omega$  is bounded, this implies  $v \in L^1(\Omega)$ . We claim the area  $\mu(S_\alpha)$  can be approximated by

$$A_\varepsilon^{(\alpha)}(v) = \int_{\Omega} \Phi_\varepsilon(v(x) - \alpha) d\mu(x).$$

**Proposition 2.** For every fixed  $v \in L^\infty(\Omega)$  and  $\alpha \in \mathbb{R}$  we have

$$\lim_{\varepsilon \downarrow 0} A_\varepsilon^{(\alpha)}(v) = \mu(\{x \in \Omega : v(x) > \alpha\}).$$

*Proof of Proposition 2.* Let  $\{\varepsilon_n\}$  be monotone decreasing to zero and  $V_{t,n} := \{x \in \Omega : v(x) \geq \alpha + \varepsilon_n t\}$ . For every fixed  $t \geq 0$  we have  $V_{t,n} \subseteq V_{t,n+1}$ . Define  $V := \bigcup_{n>0} V_{t,n} = \{x \in \Omega : v(x) > \alpha\}$  and  $h_n(t) = \varphi(t)\mu(V_{t,n})$ . Note the latter are measurable as  $t \mapsto \mu(V_{t,n})$  is monotone. Then  $h_n(t) \uparrow \varphi(t)\mu(V)$  as  $n \rightarrow \infty$  by continuity from below [40, Proposition 1.2.5]. By Fubini's theorem

$$\begin{aligned} A_{\varepsilon_n}^{(\alpha)}(v) &= \int_{\Omega} \int_{-\infty}^{v(x)-\alpha} \varphi_{\varepsilon_n}(t) dt d\mu(x) \\ &= \int \varphi_{\varepsilon_n}(t) \int_{\Omega} \chi_{\{v(x)-\alpha \geq t\}}(t, x) d\mu(x) dt \\ &= \int \varphi_{\varepsilon_n}(t) \mu(\{x \in \Omega : v(x) \geq \alpha + t\}) dt \\ &= \int_0^\infty \varphi(t) \mu(V_{t,n}) dt \\ &\xrightarrow{\varepsilon \downarrow 0} \mu(\{x \in \Omega : v(x) > \alpha\}) \end{aligned}$$

where we used the monotone convergence theorem [40, Theorem 2.4.1]. As  $\{\varepsilon_n\}$  is arbitrary, the claim follows.  $\square$

Therefore, writing  $A_\varepsilon = A_\varepsilon^{(0)}$ , we have for  $u \in W$  and  $\varepsilon$  small that

$$A_\varepsilon(Tu) = \int_{\Omega} \Phi_\varepsilon(Tu(x)) d\mu(x) \approx \mu(\{x \in \Omega : Tu(x) > 0\}) = \mu(\mathcal{S}(u)^c) = \mu(\Omega) - \mu(\mathcal{S}(u))$$

whence  $\mu(\mathcal{S}(u)) \approx \mu(\Omega) - A_\varepsilon(Tu)$ . This allows us to use directly an integral functional of a function of  $Tu$  thereby removing the need to use the set  $\mathcal{S}(u)$  as an optimization variable.

### 3.2 The variational problem

We propose to solve the  $\varepsilon$ -approximated problem

$$(P_\varepsilon) \quad \begin{cases} \text{minimize} & A_\varepsilon(Tu) \\ & u \in W_S \\ \text{subject to} & u \in \mathcal{P}. \end{cases} \quad (12)$$

We can characterize the regularity of the objective function for this problem.

**Proposition 3.** *The function  $A_\varepsilon : L^\infty(\Omega) \rightarrow \mathbb{R}$  is continuous. Since  $W_S$  is compact, there exists at least one solution to (12).*

*Proof of Proposition 3.* Let  $\delta > 0$  and  $v_0, v \in L^\infty(\Omega)$  be such that  $\|v - v_0\|_{L^\infty} < \delta/2$ . Then  $|v(x) - v_0(x)| < \delta/2$  for  $x$  on a set of full measure. Since  $\varphi(t)$  is bounded for  $-\|v_0\|_{L^\infty} - \delta/2 \leq t \leq \|v_0\|_{L^\infty} + \delta/2$  we have

$$|\Phi_\varepsilon(v(x)) - \Phi_\varepsilon(v_0(x))| \leq \int_{v_0(x)-\delta/2}^{v_0(x)+\delta/2} \varphi(t) dt \leq c_{v_0, \varphi} \delta$$

where  $c_{v_0, \varphi} > 0$  depends only on  $\varphi$  and  $v_0$ . Thus,  $|A_\varepsilon(v_2) - A_\varepsilon(v_1)| \leq c_{v_0, \varphi} \mu(\Omega) \delta$  whence  $A_\varepsilon$  is continuous. The existence of solutions follows from the compactness of  $W_S \cap \mathcal{P}$ .  $\square$

Unfortunately, we cannot assert that the solution to (12) is unique and, in fact, several solutions may exist as two distinct sound waves may be the best psycho-acoustic approximation to  $u_0$  on  $\Omega$ . Consider the case  $u_0 \equiv 0$ : any sound wave  $u \in W_S$  of sufficiently small magnitude falls below the pain and hearing thresholds, and is thus optimal for (12). In addition, although the feasible set is convex, the objective function is not. Therefore, in principle, there may not be efficient algorithms to solve (12), and several local minima may exist.

## 4 DC Formulation

To introduce a suitable algorithm to solve (12) we first rewrite it as

$$(P'_\varepsilon) \quad \begin{cases} \text{minimize} & A_\varepsilon(v) \\ & u \in W_S, v \in L^\infty(\Omega) \\ \text{subject to} & Tu \leq v, \quad u \in \mathcal{P}. \end{cases} \quad (13)$$

We interpret the auxiliary variable  $v$  as an overestimate of the threshold map over  $\Omega$ . The proof of the following proposition shows that for all practical purposes we can assume  $Tu = v$ .

**Proposition 4.** *The following assertions are true.*

- (i) *The set  $\{(u, v) : Tu \leq v\}$  is closed and convex.*
- (ii) *If  $u^*$  is an optimal solution to  $(P_\varepsilon)$  then  $(u^*, Tu^*)$  is an optimal solution to  $(P'_\varepsilon)$ . In particular,  $(P'_\varepsilon)$  has a solution.*
- (iii) *If  $(Tu^*, v^*)$  is an optimal solution to  $(P'_\varepsilon)$  then  $(u^*, Tu^*)$  is also an optimal solution, and  $u^*$  is an optimal solution to  $(P'_\varepsilon)$ .*
- (iv) *The problems  $(P_\varepsilon)$  and  $(P'_\varepsilon)$  are equivalent.*

*Proof of Proposition 4.* We omit details for brevity. (i) Convexity follows from (i) in Proposition 1. Similarly, the set is closed by the continuity of  $T$ . (ii)-(iv) Let  $u$  be an optimal solution to  $(P_\varepsilon)$ . By choosing  $v = Tu$  it is clear the optimal solution to  $(P'_\varepsilon)$  is less or equal than that of  $(P_\varepsilon)$ . Let  $(u', v')$  be an optimal solution to  $(P'_\varepsilon)$ . We claim that we can choose  $v'$  so that  $v' = Tu'$ . First, remark that  $v_1 \leq v_2$  implies that  $A_\varepsilon(v_1) \leq A_\varepsilon(v_2)$ . Therefore, we can define  $v'' \in L^\infty(\Omega)$  as  $v''(x) = \min\{v'(x), Tu'(x)\} = Tu'(x)$  whence  $A_\varepsilon(v'') \leq A_\varepsilon(v')$ . Since  $(u', v')$  is optimal,  $A_\varepsilon(v'') = A_\varepsilon(v')$  and, without loss, we can assume  $v' = Tu'$ . Consequently, the optimal value of  $(P'_\varepsilon)$  is greater or equal to that of  $(P_\varepsilon)$ . Hence the problems are equivalent and, by Proposition 3, they both have at least one solution.  $\square$

---

**Algorithm 1:** SWEET

---

**input :** A decreasing sequence  $\{\varepsilon_k\}$  of positive numbers with  $\varepsilon_0 \gg 1$ ,  $N_\varepsilon, N_u \in \mathbb{N}$  and  $v_0 \in L^\infty(\Omega)$   
**set** :  $N = N_\varepsilon N_u$   
**for**  $i = 0, \dots, N_\varepsilon - 1$  **do**  
    **for**  $j = 0, \dots, N_u - 1$  **do**  
         $k = iN_u + j$   
         $(u_{k+1}, v_{k+1})$  solution to  $(P_{\varepsilon_i, v_k})$   
    **end**  
**end**  
**return**  $u_N$

---

From now on, we denote both (12) and (13) as  $(P_\varepsilon)$  and we omit the subscript  $\varepsilon$  when possible. Note that in (13) the objective is the *difference of convex functions*. Since  $\varphi$  is of bounded variation we can consider its Jordan decomposition [41, Chapter 6, Jordan's Theorem]  $\varphi = \varphi_+ - \varphi_-$  where  $\varphi_+, \varphi_- : \mathbb{R} \rightarrow \mathbb{R}$  are non-decreasing functions which we assume to be zero for  $t < 0$ . Define

$$\Phi_+(t) = \int_{-\infty}^t \varphi_+(s) ds, \quad \Phi_-(t) = \int_{-\infty}^t \varphi_-(s) ds$$

By construction,  $\Phi = \Phi_+ - \Phi_-$ . Hence, we can decompose  $A$  as  $A = A_+ - A_-$  where

$$A_+(v) := \int_{\Omega} \Phi_+(v(x)) d\mu(x), \quad A_-(v) := \int_{\Omega} \Phi_-(v(x)) d\mu(x).$$

**Proposition 5.** *The functions  $A_+, A_- : L^\infty(\Omega) \rightarrow \mathbb{R}$  are convex and continuous.*

*Proof of Proposition 5.* By construction, both  $\Phi_+$  and  $\Phi_-$  have a derivative almost everywhere that is non-decreasing, hence monotone [42, Proposition 17.10]. Therefore  $\Phi_+$  and  $\Phi_-$  are convex. With this, and the linearity and monotonicity of the integral,  $A_+$  and  $A_-$  are convex. Moreover, they are continuous as the proof of Proposition 3 holds *mutatis mutandis*.  $\square$

Hence, the formulation (13) is a Difference-of-Convex (DC) program [43, 44]. For this type of problems, there are efficient algorithms that attempt to find a solution.

#### 4.1 SWEET algorithm

The Convex-Concave Procedure (CCCP) [45] is an efficient method, which can be thought as a primal version of the DCA algorithm [43], to find a solution to (13). Although it can be shown that if it converges, then its limit is a stationary point [43, Theorem 3], our results in Section 6 suggest that in practice we are able to find local minima for (13). The CCCP is an iterative method that uses an affine majorant for the concave part, e.g., using subgradients, to then majorize the objective function in (13) with a convex function. The resulting convex problem can then be solved efficiently.

Since  $A_-$  is continuous and convex, it has a subdifferential  $\partial A_-(v_0) \subset L^\infty(\Omega)'$  at every  $v_0 \in L^\infty(\Omega)$  [46, Proposition 2.36]. If  $g \in \partial A_-(v_0)$  then

$$A_-(v) \geq A_-(v_0) + g(v - v_0)$$

for any  $v \in L^\infty(\Omega)$ . The functional  $g$  is called a subgradient. Therefore, we can use the convex majorizer

$$A(v) = A_+(v) + A_-(v) \leq A_+(v) - A_-(v_0) - g(v - v_0).$$

Although it may be difficult to characterize the subdifferential of a convex function on a Banach space, in our case we can always find at least a subgradient at any  $v_0$ .

**Proposition 6.** *Let  $v_0 \in L^\infty(\Omega)$ . Then*

$$g_{v_0}(v) = \int_{\Omega} \varphi_-(v_0(x)) v(x) d\mu(x) \tag{14}$$

*is a subgradient for  $A_-$  at  $v_0$ .*

*Proof of Proposition 6.* Let  $v \in L^\infty(\Omega)$ ,  $t, t_0 \in \mathbb{R}$ . By the monotonicity of  $\varphi_-$  we have

$$\Phi_-(t_0) + \varphi_-(t_0)(t - t_0) = \int_{-\infty}^{t_0} \varphi_-(s)ds + \int_{t_0}^t \varphi_-(t_0)ds \leq \int_{-\infty}^t \varphi_-(s)ds = \Phi_-(t).$$

Since  $t \in \mathbb{R}$  is arbitrary,  $\varphi_-(t_0)$  is a subgradient of  $\Phi_-$  at  $t_0$ . Moreover, since  $t_0 \in \mathbb{R}$  is arbitrary, we have that

$$(\Phi_- \circ v_0) + (\varphi_- \circ v) \cdot (v - v_0) \leq (\Phi_- \circ v).$$

Whence, by the monotonicity of the integral, integrating over  $\Omega$  yields

$$A_-(v) \geq A_-(v_0) + \int_{\Omega} \varphi_-(v_0(x))(v(x) - v_0(x)) d\mu(x).$$

Since  $v \in L^\infty(\Omega)$  is arbitrary,  $g_{v_0}$  is a subgradient of  $A_-$  at  $v_0$ .  $\square$

The CCCP solves at each iteration the convex problem

$$(P_{\varepsilon, v_0}) \begin{cases} \text{minimize} & A_+(v) - A_-(v_0) - g_{v_0}(v - v_0) \\ u \in W_S, v \in L^\infty(\Omega) \\ \text{subject to} & Tu \leq v, \quad u \in \mathcal{P}. \end{cases} \quad (15)$$

The proof of Proposition 3 can be adapted to show  $(P_{\varepsilon, v_0})$  has at least one solution.

**Proposition 7.** *There exists at least one solution to (15).*

*Proof of Proposition 7.* We first construct a candidate for an unconstrained minimizer of the objective. Let  $\tilde{v}_0$  be any representative of  $v_0 \in L^\infty(\Omega)$ . Define the set-valued map  $F : \Omega \rightrightarrows \mathbb{R}$  as

$$F(x) := \arg \min \{ \Phi_+(t) - \varphi_-(\tilde{v}_0(x))t : t \in \mathbb{R} \}.$$

Let  $\Omega_+ := \{x \in \Omega : \varphi_-(\tilde{v}_0(x)) > 0\}$ . Since  $\varphi_-$  vanishes on the negative reals, if  $x \notin \Omega_+$  then  $\varphi_-(\tilde{v}_0(x)) = 0$ . Furthermore, since  $\Phi_+$  takes non-negative values and vanishes on the non-positive reals, it is clear that  $F(x) \supset (-\infty, 0]$  for  $x \notin \Omega_+$ .

Assume  $x \in \Omega_+$ . Let  $t \geq \tilde{v}_0(x)$ . Since  $\varphi_+ - \varphi_- \geq 0$  and both  $\varphi_+, \varphi_-$  are non-decreasing, we deduce that  $\varphi_+(t) - \varphi_-(\tilde{v}_0(x)) \geq 0$ . Since  $\varphi_+(t) \in \partial\Phi_+(t)$  the latter inequality implies  $F(x) \subset (-\infty, \tilde{v}_0(x)]$ . Let  $t < 0$ . Then, the objective is differentiable with derivative  $-\varphi_-(\tilde{v}_0(x)) < 0$ . Hence,  $F(x) \subset [0, v_0(x)]$  for  $x \in \Omega_+$ . In particular,  $F$  takes non-empty, closed and convex values on a complete metric space. Therefore, it admits a measurable selection  $\tilde{v}^*$  [47, Theorem 8.2.2 and Theorem 8.1.13]. Note that  $|\tilde{v}^*(x)| \leq |\tilde{v}_0(x)|$  for  $x \in \Omega_+$ . With a slight abuse of notation, we denote  $\tilde{v}^*$  its extension by zero to all of  $\Omega$ . Note this is still a measurable selection for  $F$ . If we let  $v^*$  denote its equivalence class, we deduce that  $\|v^*\|_{L^\infty} \leq \|v_0\|_{L^\infty}$  whence  $v^* \in L^\infty(\Omega)$ .

By construction, for any  $v \in L^\infty(\Omega)$  and representative  $\tilde{v}$  of  $v$  we have

$$\Phi_+(\tilde{v}(x)) - \varphi_-(\tilde{v}_0(x))\tilde{v}(x) \geq \Phi_+(\tilde{v}^*(x)) - \varphi_-(\tilde{v}_0(x))\tilde{v}^*(x)$$

whence

$$A_+(v) - g_{v_0}(v) \geq A_+(v^*) - g_{v_0}(v^*).$$

Consequently,  $v^*$  is indeed an unconstrained minimizer for the objective.

We now prove a minimizer exists. Let  $\{(u_k, v_k)\}$  be a minimizing sequence. Since  $W_S$  is compact by Proposition 1, we can assume without loss that  $\{u_k\}$  converges to a limit  $u_\infty \in W_S$ . Define  $w_k = \max\{v^*, Tu_k\}$ . We will show  $\{(u_k, w_k)\}$  is also minimizing. Define  $\Omega_k := \{x \in \Omega : Tu_k(x) = w_k(x)\}$ . Since  $v_k$  is feasible, we have  $v^*|_{\Omega_k} \leq Tu_k|_{\Omega_k} \leq v_k|_{\Omega_k}$ . Then, for almost every  $x \in \Omega_k$  we have

$$\Phi_+(v_k(x)) - \varphi_-(v_0(x))v_k(x) \geq \Phi_+(Tu_k(x)) - \varphi_-(v_0(x))Tu_k(x) \geq \Phi_+(v_k^*(x)) - \varphi_-(v_0(x))v_k^*(x)$$

by construction. By applying the same arguments as in the proof of Proposition 6, we obtain the inequality

$$\int_{\Omega_k} (\Phi_+(v_k(x)) - \varphi_-(v_0(x))v_k(x))d\mu(x) \geq \int_{\Omega_k} (\Phi_+(Tu_k(x)) - \varphi_-(v_0(x))Tu_k(x))d\mu(x).$$

From this, it follows that

$$A_+(v_k) - g_{v_0}(v_k) \geq A_+(w_k) - g_{v_0}(w_k).$$

Hence,  $(u_k, w_k)$  attains a lower objective value than  $(u_k, v_k)$ . Since  $\{(u_k, v_k)\}$  is minimizing, we conclude

$$p^* = \liminf_{k \rightarrow \infty} (A_+(v_k) - g_{v_0}(v_k)) \geq \liminf_{k \rightarrow \infty} (A_+(w_k) - g_{v_0}(w_k)) \geq p^*$$

where  $p^*$  is the optimal value; hence,  $\{(u_k, w_k)\}$  is also minimizing. Since  $T$  is continuous, we have  $w_k \rightarrow \max\{v^*, Tu_\infty\}$ . Hence,  $(u_\infty, \max\{v^*, Tu_\infty\})$  is a minimizer.  $\square$

By solving a sequence of problems of the form  $(P_{\varepsilon, v_{k+1}})$ , where  $(u_{k+1}, v_{k+1})$  is an optimal solution to  $(P_{\varepsilon, v_k})$ , we can attempt to find a solution to  $(P_{\varepsilon})$ .

Assuming the CCCP converges to a local minimizer to  $(P_{\varepsilon})$ , we can then solve a sequence of problems of the form  $(P_{\varepsilon_k})$  for a decreasing sequence  $\{\varepsilon_k\}$  to approximate a solution to  $(P_0)$ . In this case, we initialize the CCCP to solve  $(P_{\varepsilon_{k+1}})$  with the solution found for  $(P_{\varepsilon_k})$ . We call this the SWEET algorithm and is shown in Algorithm 1.

Finally, remark we could apply the decomposition  $A \circ T = A_+ \circ T - A_- \circ T$  in (12). Although the term  $A_- \circ T$  is convex when  $\phi_+ \geq 0$ , majorizing  $-A_- \circ T$  would be more involved than the approach we have taken here.

## 4.2 SWEET-ReLU algorithm

When  $\varphi$  is a step function, the function  $\Phi$  is the difference of two *Rectified Linear Units* (ReLU). The resulting instance of Algorithm 1 is simple and interpretable. Let  $\varepsilon > 0$  and  $\varphi = \varepsilon^{-1}\chi_{[0, \varepsilon]}$ . Choosing  $\varphi_+ = \varepsilon^{-1}\chi_{[0, \infty)}$  and  $\varphi_- = \varepsilon^{-1}\chi_{[\varepsilon, \infty)}$ , the decomposition  $\Phi = \Phi_+ - \Phi_-$  becomes

$$\Phi(x) = \frac{1}{\varepsilon}(x_+ - (x - \varepsilon)_+)$$

whence  $\Phi_+$  and  $\Phi_-$  are ReLUs. Moreover, the subgradient (14) becomes

$$g_{v_0}(v) = \frac{1}{\varepsilon} \int_{\{x: v_0(x) > \varepsilon\}} v(x) d\mu(x).$$

Let  $\Omega_{\varepsilon, v_0} := \{x : v_0(x) \leq \varepsilon\}$ . Since  $A_-(v_0)$  and  $g_{v_0}(v_0)$  in  $(P_{\varepsilon, v_0})$  the terms are constant, it suffices to compute

$$\begin{aligned} A_+(v) - g_{v_0}(v) &= \frac{1}{\varepsilon} \int_{\Omega} v(x)_+ d\mu(x) - \frac{1}{\varepsilon} \int_{\Omega_{\varepsilon, v_0}^c} v(x) d\mu(x) \\ &= \frac{1}{\varepsilon} \int_{\Omega_{\varepsilon, v_0}} v(x)_+ d\mu(x) + \frac{1}{\varepsilon} \int_{\Omega_{\varepsilon, v_0}^c} (-v(x))_+ d\mu(x) \end{aligned}$$

where we used the fact that  $t_+ - t = (-t)_+$ . The second term is non-negative, and it is positive only when  $v$  takes negative values. The restriction  $Tu \leq v$  in  $(P_{\varepsilon, v_0})$  allows us to choose  $v$  arbitrarily large over  $\Omega_{\varepsilon, v_0}^c$ , decreasing the objective value, and allowing us to neglect the second integral. Therefore, only the first term contributes to the objective in  $(P_{\varepsilon, v_0})$ . Hence, for this choice of  $\varphi, \varphi_+$  and  $\varphi_-$  we obtain

$$(P_{\varepsilon, v_0}) \quad \begin{cases} \text{minimize} & \int_{\Omega_{\varepsilon, v_0}} v(x)_+ d\mu(x) \\ \text{subject to} & u \in \mathcal{P} \\ & Tu \leq v, 0 \leq v|_{\Omega_{\varepsilon, v_0}^c}. \end{cases} \quad (16)$$

Because of the monotonicity of the positive-part function we can eliminate the auxiliary variable  $v$  to obtain the problem

$$(P_{\Omega_{\varepsilon, v_0}}^{ReLU}) \quad \begin{cases} \text{minimize} & \int_{\Omega_{\varepsilon, v_0}} (Tu(x))_+ d\mu(x) \\ \text{subject to} & u \in \mathcal{P}. \end{cases} \quad (17)$$

Note it depends on  $v_0$  only through the set  $\Omega_{\varepsilon, v_0}$ . With this in mind, notice that at each iteration of Algorithm 1 we need an optimal solution  $(u_{k+1}, v_{k+1})$  to  $(P_{\varepsilon, v_k})$ . However, solving (17) only yields an optimal solution  $u_{k+1}$ . Fortunately, from a given solution  $u_{k+1}$  to (17) we can choose  $v_{k+1}$  such that  $(u_{k+1}, v_{k+1})$  is an optimal solution to (16) as follows: let  $v_{k+1}|_{\Omega_{\varepsilon, v_k}} = Tu_{k+1}|_{\Omega_{\varepsilon, v_k}}$  and  $v_{k+1}|_{\Omega_{\varepsilon, v_k}^c} = \max\{\varepsilon, Tu_{k+1}|_{\Omega_{\varepsilon, v_k}^c}\}$ . Using this choice, note that

$$\begin{aligned} \Omega_{\varepsilon, v_{k+1}} &= \{x : v_{k+1}(x) \leq \varepsilon\} \\ &= \{x \in \Omega_{\varepsilon, v_k} : Tu_{k+1}(x) \leq \varepsilon\} \\ &= \Omega_{\varepsilon, v_k} \cap \{x \in \Omega : Tu_{k+1}(x) \leq \varepsilon\}. \end{aligned}$$

We call this simplification the SWEET-ReLU algorithm. It is shown in Algorithm 2. Due to compactness, the iterates  $\{u_k\}$  have at least one accumulation point, which must be a stationary point for (12) [43, Theorem 3]. SWEET-ReLU can be interpreted as a *greedy algorithm* that improves at each step the approximation over the set  $\Omega_k$  while neglecting the approximation outside  $\Omega_k$ . Intuitively, a point in  $\Omega$  is neglected by the algorithm as soon as it determines that it cannot belong to the sweet spot. Furthermore, the sequence of sets generated by the algorithm are precisely an approximation for the sweet spot as, in fact,  $\mathcal{S}(u_N) \approx \Omega_N$ . Additionally, initializing the algorithm with  $\varepsilon_0$  sufficiently large we have  $\Omega_1 = \Omega$ , making the choice of  $u_0$  irrelevant. Finally, the choice of  $\{\varepsilon_i\}$  can be adaptive. For instance,  $\varepsilon_i$  can be selected as the  $p$ -th percentile of  $Tu_{iN_u - 1}$ .

---

**Algorithm 2:** SWEET-ReLU

---

**input:** A decreasing sequence  $\{\varepsilon_i\}$  of positive numbers with  $\varepsilon_0 \gg 1$ ,  $N_\varepsilon, N_u \in \mathbb{N}$ ,  $u_0 \in W$  and  $\Omega_0 = \Omega$   
**set** :  $N = N_\varepsilon N_u$   
**for**  $i = 0, \dots, N_\varepsilon - 1$  **do**  
    **for**  $j = 0, \dots, N_u - 1$  **do**  
         $k = iN_u + j$   
         $\Omega_{k+1} = \Omega_k \cap \{x \in \Omega : Tu_k(x) \leq \varepsilon_i\}$   
         $u_{k+1}$  solution to  $(P_{\Omega_{k+1}}^{ReLU})$   
    **end**  
**end**  
**return**  $u_N$

---

## 5 Implementation

We provide an implementation of SWEET-ReLU for approximating a sound wave generated by a (pseudo) sinusoidal isotropic point source emitting at frequencies  $f_1^*, \dots, f_{n_f}^*$ . The loudspeakers are modeled as equivalent (pseudo) sinusoidal point sources, i.e. we use

$$\widehat{c}_k(f) = \sum_{\ell=1}^{n_f} a_{k,\ell} e^{-(f-f_\ell^*)^2/2\sigma^2}$$

in (1) for coefficients  $a_{k,\ell} \in \mathbb{C}$  and a fixed spectral localization parameter  $\sigma \ll 1$ . Since the signals are almost stationary, temporal masking is almost non-existent. This allows us to define the threshold map  $T$  using van de Par's spectral psycho-acoustic model [25]. In this case, the filters in (8) are time-invariant. Thus, for van de Par's model we have

$$B_j u(x) = \int |\widehat{u} - \widehat{u}_0|(f, x)|^2 \rho_{B_j}(f, x) df$$

for

$$\rho_{B_j}(f, x) = \frac{w_{B_j}(f)}{C_A + \int |\widehat{u}_0(f, x)|^2 w_{B_j}(f) df}.$$

The constant  $C_A > 0$  limits the perception of very weak signals in silence. The weight  $w_{B_j}$  is defined as  $w_{B_j} := |\eta\gamma_j|^2$  where

$$\log_{10} \eta(f) = C_{\eta,0} - C_{\eta,1} f^{-0.8} - C_{\eta,2} (f - 3.3 \times 10^3)^2 + C_{\eta,3} f^4$$

with  $C_{\eta,0} = 4.69$ ,  $C_{\eta,1} = 18.2 \times 10^{1.4}$ ,  $C_{\eta,2} = 32.5 \times 10^{-7}$  and  $C_{\eta,3} = 5 \times 10^{-16}$  models the outer and middle ear as proposed by Terhardt [48], and

$$\gamma_j(f) = \left( 1 + \left( \frac{945\pi(f - f_j)}{48\text{ERB}(f_j)} \right)^2 \right)^{-2}$$

models the filtering property of the basilar membrane in the inner ear at the center frequency  $f_j$ , where the Equivalent Rectangular Bandwidth (ERB) of the auditory filter centered at  $f_j$  is  $\text{ERB}(f_j) = 24.7(1 + 4.37 \times 10^{-3} f_j)^{-1}$  as suggested by Glasberg and Moore [49]. The center frequencies  $f_j$  are uniformly spaced on the ERB-rate scale  $\text{ERBS}(f) = 21.4 \log(1 + 4.37 \times 10^{-3} f)$ . For  $n_b$  center frequencies  $f_j$  we obtain  $n_b$  maps  $B_j$  that are combined with the integrating function  $\Psi(b_1, \dots, b_{n_b}) = -1 + C_\Psi b_1 + \dots + C_\Psi b_{n_b}$  for a suitable constant  $C_\Psi > 0$ . The threshold map becomes

$$\begin{aligned} Tu(x) &= -1 + C_\Psi \sum_{j=1}^{n_b} \frac{\int |\widehat{u}(f, x) - \widehat{u}_0(f, x)|^2 w_{B_j}(f) df}{C_A + \int |\widehat{u}_0(f, x)|^2 w_{B_j}(f) df} \\ &\approx -1 + C'_\Psi \sum_{\ell=1}^{n_f} \sum_{j=1}^{n_b} \frac{|\widehat{u}(f_\ell^*, x) - \widehat{u}_0(f_\ell^*, x)|^2 w_{B_j}(f_\ell^*)}{C_A + w_{B_j}(f_\ell^*) |\widehat{u}_0(f_\ell^*, x)|^2} \end{aligned}$$

where  $C'_\Psi = 2^{1/4} \pi^{1/2} \sigma C_\Psi$  and we used the approximation for (pseudo) sinusoidal signals

$$\int \varphi(f) |\widehat{u}_0(f, x)|^2 df \approx 2^{1/4} \pi^{1/2} \sigma \sum_{\ell=1}^{n_f} \varphi(f_\ell^*) |\widehat{u}_0(f_\ell^*, x)|^2$$

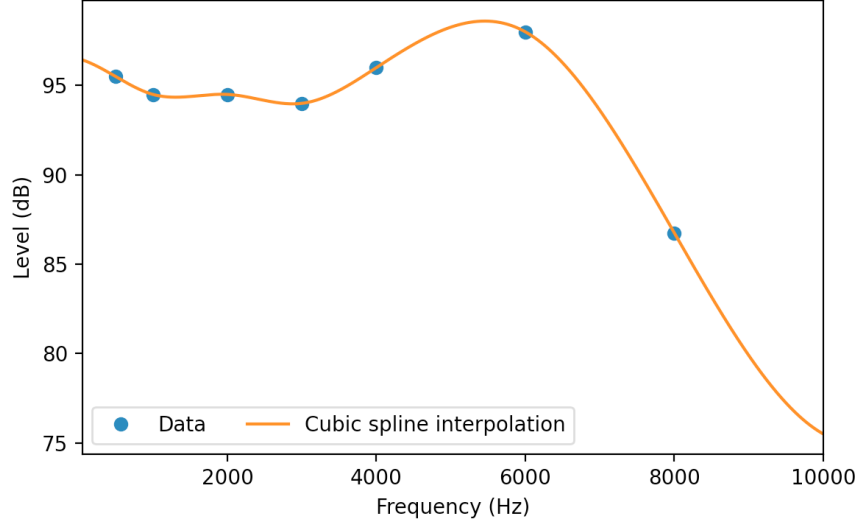


Figure 2: Interpolation of the loud discomfort levels for sinusoidal signals given in (Knobel & Sanchez, 2006) by cubic splines.

when  $\sigma \ll 1$ . The constants  $C'_\Psi$  and  $C_A$  are defined as suggested in [25]. This considers the absolute threshold of hearing and the just-noticeable difference in level for sinusoidal signals, which gives,  $C'_\Psi \approx 1.555$  and  $C_A \approx 4.481$  when considering  $n_b = 100$  as the number of center frequencies, and  $f_1 = 20$ ,  $f_{n_b} = 10^3$  as the first and last center frequency.

To model the pain threshold we consider the experiments in [37] about the discomfort caused by sinusoidal signals. We interpolated the data in this study using cubic splines with natural boundary [50, Section 8.6] to obtain a function  $\eta_P$ , as shown in Fig. 2. For the auditory filter associated to the  $j$ -th frequency we define

$$\rho_{Q_j}(f, x) = |w_{Q_j}(f)/\eta_P(f)|^2$$

To our knowledge, there is no standard reference for the spectral integration that determines the levels of discomfort or pain. For simplicity, we consider, as in the van de Par model, a summing integrating function, but now with the center frequencies of the discomfort auditory filters equal to the sound frequencies  $f_1^*, \dots, f_{n_b}^*$ . Then,  $\Pi(q_1, \dots, q_{n_f}) = -1 + C_\Pi q_1 + \dots + C_\Pi q_{n_f}$ . This is actually a conservative choice of  $\Pi$  as this controls the sum of the contributions of every frequency, instead of each one separately. Consequently, we obtain

$$\begin{aligned} Pu(x) &= -1 + C_\Pi \sum_{\ell=1}^{n_f} \int |\hat{u}(f, x)|^2 \rho_{Q_\ell}(f, x) df \\ &\approx -1 + C'_\Pi \sum_{\ell=1}^{n_f} |\hat{u}(f_\ell^*, x)|^2 \rho_{Q_\ell}(f_\ell^*, x) \end{aligned}$$

where the same approximation holds by the same arguments as before. Naturally,  $C'_\Pi = 1$ .

To solve  $(P_{\Omega_\varepsilon, v_0}^{ReLU})$  we discretize the integrals over  $\Omega$ . The following proposition ensures that this approximation to the integral converges to the desired one under mild assumptions. We defer its proof to Appendix B.

**Proposition 8.** *Suppose that the statements (i) and (ii) in Proposition 1 hold. Define for  $K \in \{K_{B_1}, \dots, K_{B_{n_b}}\}$  the function*

$$f_K(t, t') := \sup_{x \in \Omega} |K(t, t', x)|.$$

*If  $f_K \in L^2(\mathbb{R}^2)$  and  $u \in W_S$  then  $Tu \in C(\Omega)$ . Furthermore, if  $\Omega$  is compact,  $Tu$  is uniformly continuous over  $\Omega$ .*

Specifically, we discretize  $\Omega$  using  $n_d$  disjoint squares or cubes of side  $(|\Omega|/n_d)^{1/d}$  for  $d \in \{2, 3\}$ . To avoid spatial aliasing, we need at least 2 points per spatial wavelength  $\lambda_f = c_s/f$  for each frequency  $f$  of the source. This implies  $(|\Omega|/n_d)^{1/d} < \lambda_f/2$  whence  $n_d > (2/\lambda)^d |\Omega|$ . To ensure the method performs well, we typically consider a denser discretization with at least 5 points per spatial wavelength.

## 6 Experiments

We perform two types of numerical experiments. First, we compare the performance of our method with the state-of-the-art methods WFS, NFC-HOA and  $L^2$ -PMM in terms of the size of the sweet spot they produce. Second, we explore other applications of our method related to sound field reconstruction. The setup for the numerical experiments consists of an equispaced arrangement of 20 loudspeakers lying on a circle of radius 2.5 m and at  $\pi/4 \approx 0.785$  m from each other. The region of interest  $\Omega$  is a concentric circle of radius 2.4975 m (Fig. 4). The speed of sound is  $c_s = 343$  m/s.

The SWEET-ReLU algorithm and the  $L^2$ -PMM method were implemented in Python 3.8 using the CVXPY package [51, 52] and MOSEK [53]. The simulations of 2.5D NFC-HOA and 2.5D WFS were done with the SFS Toolbox [54]. To compare the results of these methods, we compare the size of the sweet spot as a fraction of the area  $|\Omega|$  of  $\Omega$ . To compare the values of the threshold map  $Tu$  for  $u$  we use  $\log(1 + Tu)$ . Hence, the sweet spot is the region where  $\log(1 + Tu) \leq 0$ . Finally, we compare the Intensity Direction Error (IDE), defined as

$$\text{IDE}u(x) = \frac{1}{\pi} \arccos \left( \frac{\vec{I}u(x)}{|\vec{I}u(x)|} \cdot \frac{\vec{I}u_0(x)}{|\vec{I}u_0(x)|} \right),$$

where  $\vec{I}$  is the time averaged acoustic intensity. For sinusoidal signals of frequency  $f^*$  it is given by [29, Section 2.3]

$$\vec{I}u(x) = \frac{1}{2} \text{Re}(u(f^*, x) \vec{v}(f^*, x)^*)$$

where  $\vec{v}$  is the velocity vector field of  $u$ .

### 6.1 Comparison with state-of-the-art methods

To compare our method with state-of-the-art methods, we perform two types of numerical experiments. The first type consists of a sequence of instances where the source moves progressively away from the center of the loudspeaker array, starting at 0 m and ending at 15 m. Following the model in Section 5, the source is isotropic, and (pseudo) sinusoidal with  $f_1^* = 343$  Hz. Hence, its wavelength is 1 m. When the source is inside  $\Omega$ , its intensity is selected so that the wave has an amplitude of 60 dB at 1 m of the source. When the source is outside  $\Omega$  we adjust the intensity so that the amplitude at the point where the segment joining the center of the arrangement and the source intersects the arrangement is 60 dB. This mitigates the effect of attenuation as the source moves away from the arrangement. A uniform discretization of 901 points was used for  $\Omega$  at a distance of at most 0.145 m, achieving more than 6 points per wavelength.

The second type considers the same source at a distance of 5 m from the center of the array emitting a (pseudo) sinusoidal wave at different frequencies ranging from 50 Hz to 2000 Hz. To mitigate the issues due to non-convexity, we initialize SWEET-ReLU with the optimal solution obtained for the previous frequency value. A uniform discretization of 20848 points was used for  $\Omega$  at a distance of at most 0.03 m, achieving more than 5 points per wavelength in the worst case. For both types of experiments we have chosen  $\varepsilon_i$  adaptively with percentile  $p = 90$ . The results are shown in Fig. 3. We see our method generates a larger sweet spot than that generated by every other method over the entire range of source locations and frequencies (Fig. 3a and Fig. 3b). When the source is at 2.5 m, lying over the arrangement, the sweet spot equals  $\Omega$ , as expected (Fig. 3a). Furthermore, our method successfully attains the lowest average threshold value in most of the instances. Although the performance degrades at very low frequencies compared to other methods, it remains below the audible threshold (Fig. 3c and Fig. 3d). This shows that on average the SWEET-ReLU algorithm does not produce large values of the threshold map outside the sweet spot.

	SWEET	NFC-HOA	WFS	$L^2$ -PMM
NF	64%	32%	35%	0.7%
FS	48%	5%	0.02%	0.5%

Table 1: Sweet spots as a fraction of  $\Omega$  in Near field (NF) and Focus Source (FS) instances.

To perform a finer analysis, we consider two additional instances: the *near-field instance*, where the source is outside the arrangement at 5 m of its center, and the *focus-source instance*, where the source is inside the arrangement at 0.82 m of its center (Fig. 4). For these experiments we have chosen  $\varepsilon_i$  adaptively with percentile  $p = 99$ . The sweet spots generated by each method for each instance are shown in Fig. 6, 8, and their size is shown in Table 1. For the near field instance, the sweet spot generated by our method is almost twice as large as that of the other methods. The sweet spot generated by NFC-HOA (Fig. 6f) is centered, whereas that generated by WFS (Fig. 6f) is localized farther away from the source. This is consistent with the analysis in [7]. In contrast, the sweet spot generated by our method

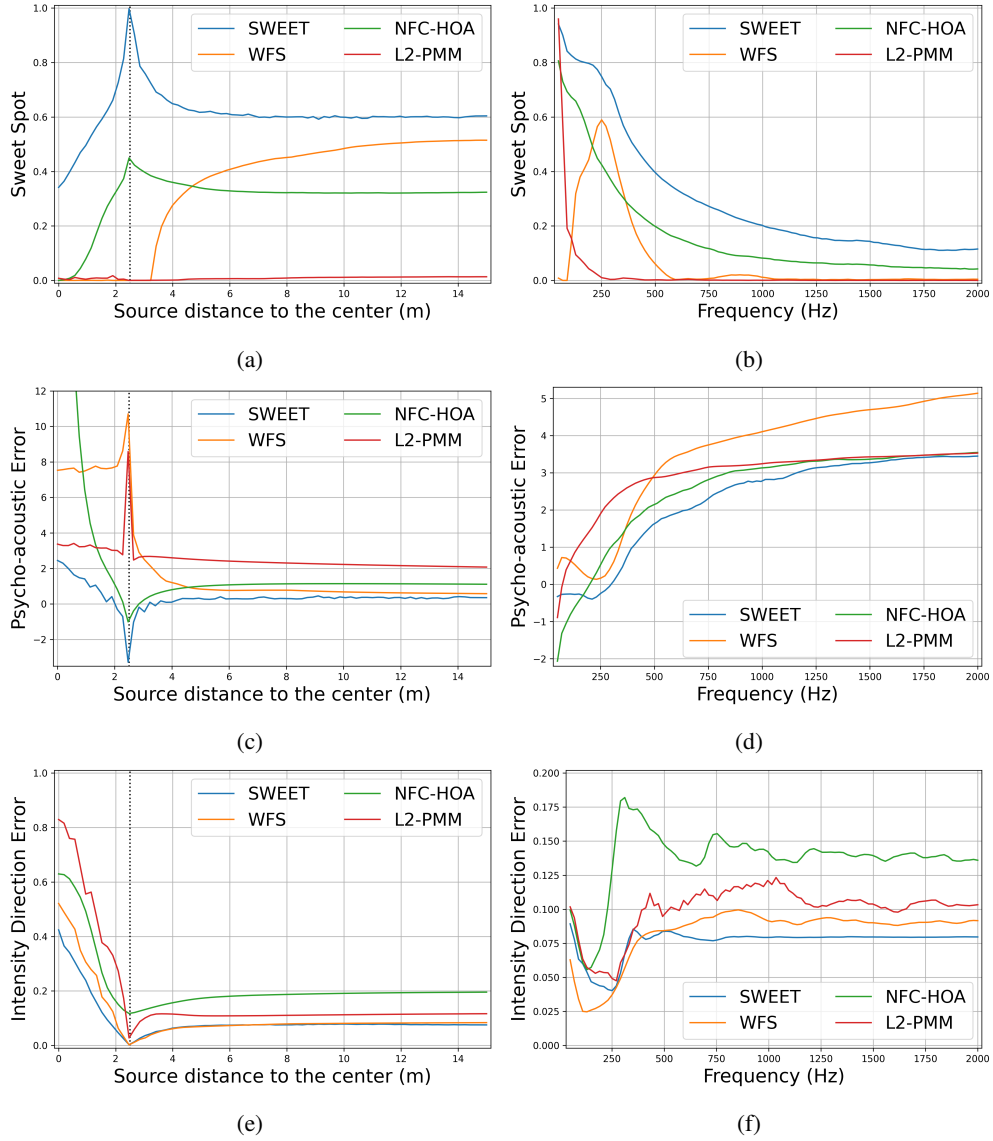


Figure 3: Comparison with state-of-the-art methods. *Columns:* (i) Variation of the distance between the source and the center of the arrangement, (ii) Variation of the frequency of the source. *Rows:* (i) Sweet spot as a fraction of  $\Omega$ , (ii) Average value for  $\log(1 + Tu)$ , (iii) Average IDE.

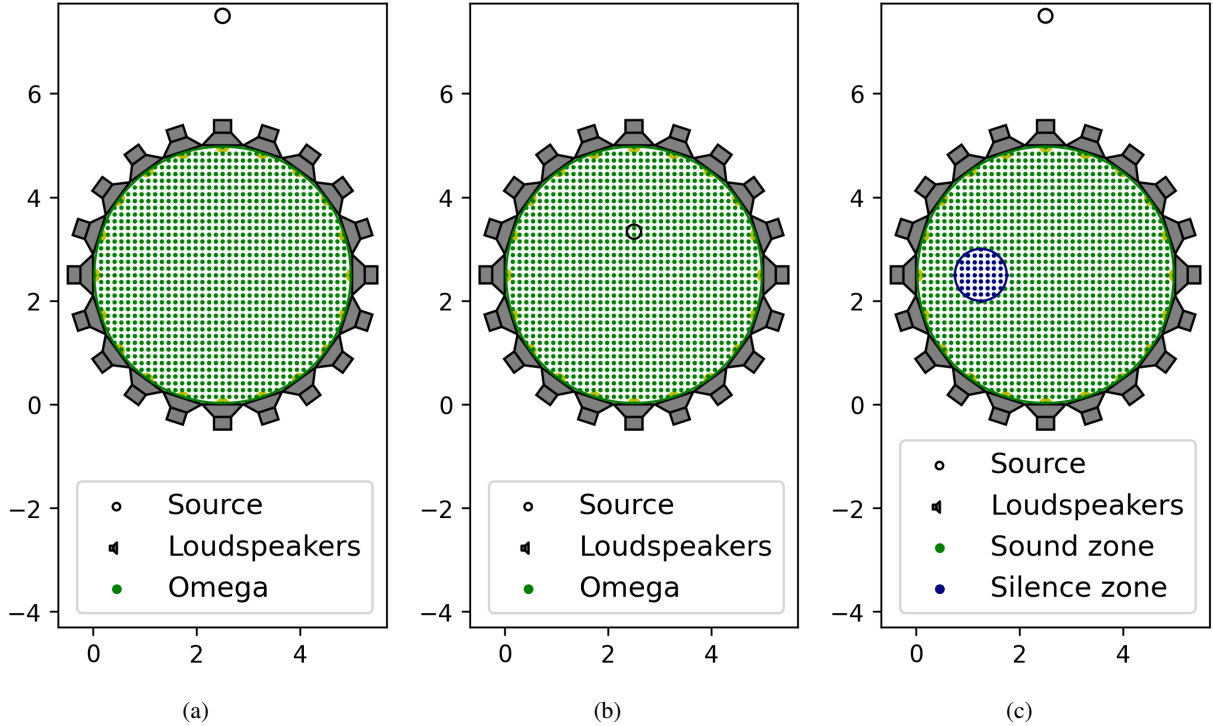


Figure 4: Experimental setup. (a) Near field setup. (b) Focus source setup. (c) Multiple zone setup.

(Fig. 6e) behaves like that generated by WFS, but almost encompasses the one generated by NFC-HOA. In all cases the aliasing artifacts appear roughly near the boundary of the sweet spot. This suggests that the principle behind sound field reconstruction, i.e., to avoid physically noticeable artifacts, does ensure a good monaural auditory scene. Our method exhibits less aliasing artifacts than the others. This may explain the low average IDE values and small psycho-acoustic errors in Fig. 3.

For the focus-source instance we strengthen the intensity of the source so that the wave has an amplitude of 72 dB at 1 m of the source. The sweet spot generated by our method (Fig. 8e) is almost 10 times larger than those generated by other methods. The sweet spot generated by NFC-HOA (Fig. 8f) is contained in a circle with a radius equal to the distance of the source to the center of the room. This is also consistent with [7]. The sweet spot generated by WFS (Fig. 8g) is almost empty as the resulting  $u$  has large amplitude. This suggests that focus source formulation for WFS needs an amplitude factor normalization. In contrast, the sweet spot generated by our method almost comprises the half of  $\Omega$  that faces the source. Furthermore, the artifacts are noticeable only behind the source. This shows the advantages of the greedy strategy of the SWEET-ReLU algorithm: during its first iterations it is capable to detect the direction of  $u_0$  over  $\Omega$  to then prioritize the part of  $\Omega$  where a good fit to  $u_0$  can be obtained. This is a possible explanation for the almost empty sweet spot generated by  $L^2$ -PMM both in the near field (Fig. 6h) and the focus source (Fig. 8h) instances. This,

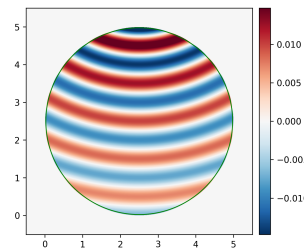


Figure 5:  $u_0$  for near field setup.

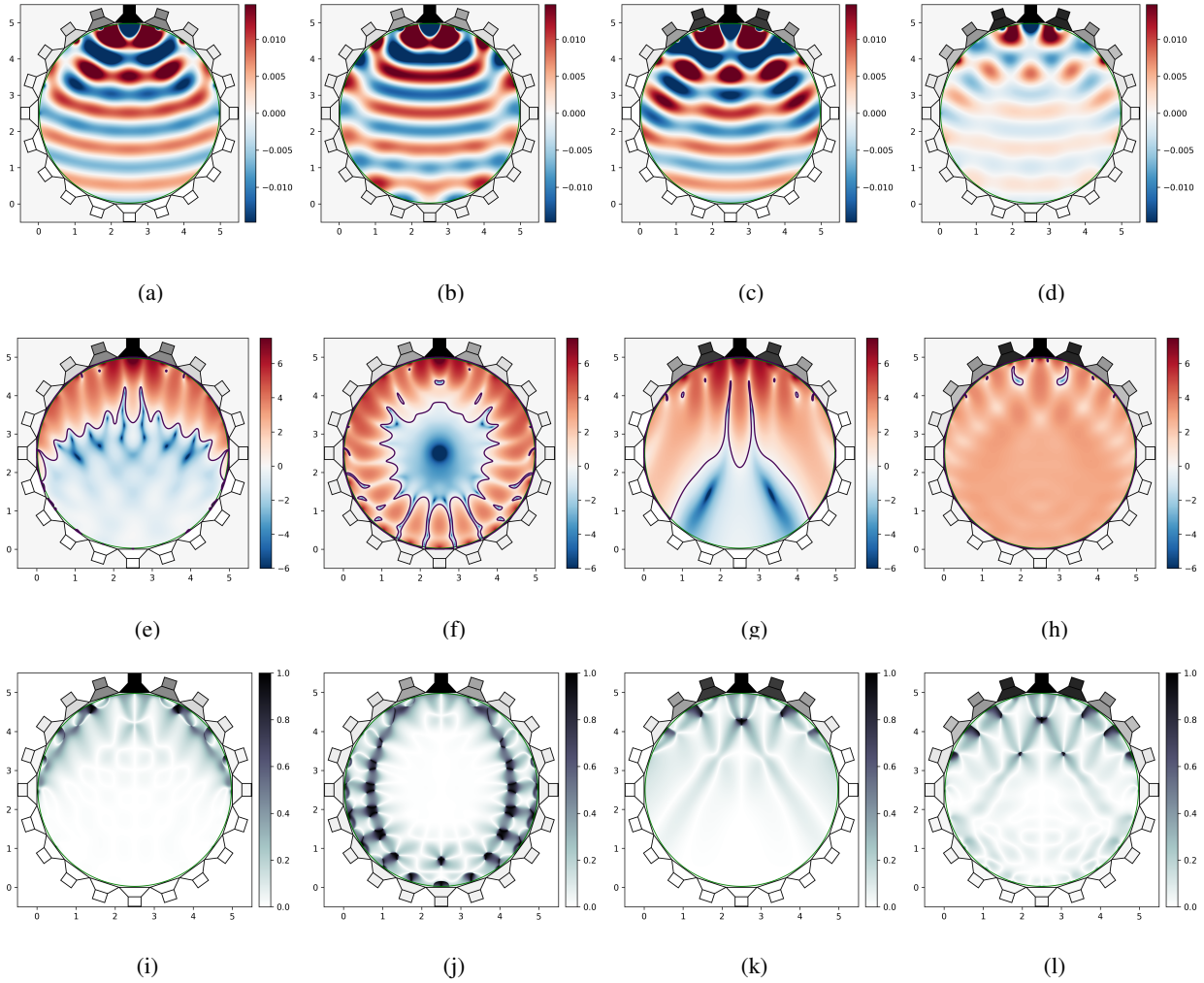


Figure 6: Near field instance. Rows: (i)  $u$ , (ii)  $\log(1 + Tu)$ , (iii) IDE. Columns: (i) SWEET-ReLU, (ii) NFC-HOA, (iii) WFS, (iv)  $L^2$ -PMM.

together with the proximity of the speakers, completely degrades its performance: the method attempts to minimize the  $L^2$ -error where it is largest, i.e., near the speakers. As a consequence, the resulting  $u$  is small over  $\Omega$ . Finally, our method is efficient in the usage of the loudspeakers: the acoustic wave  $u$  resulting from WFS is uncomfortably loud around the source and near the active loudspeakers in the array, whereas that obtained with NFC-HOA  $u_0$  is

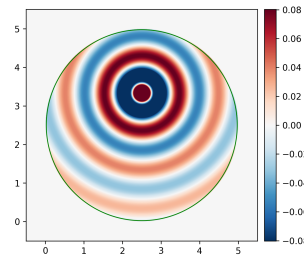


Figure 7:  $u_0$  for focus source setup.

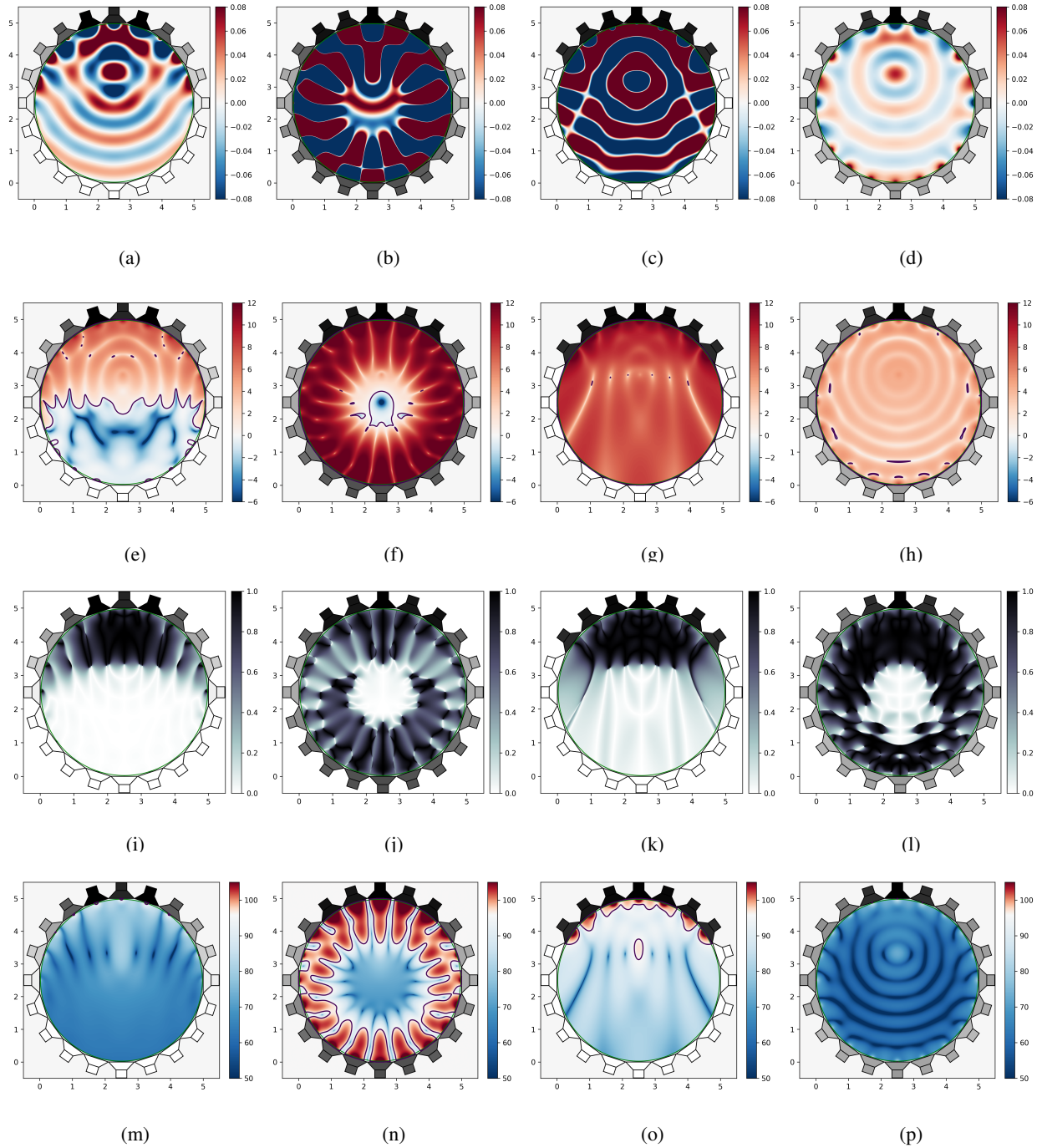


Figure 8: Focus source instance. Rows: (i)  $u$ , (ii)  $\log(1 + Tu)$ , (iii) IDE, (iv) Sound level (dB). Columns: (i) SWEET-ReLU, (ii) NFC-HOA, (iii) WFS, (iv)  $L^2$ -PM.

uncomfortably loud in a large region outside a circumference concentric to  $\Omega$ . Our method, in contrast, produces a negligible discomfort region by construction.

## 6.2 Applications

### 6.2.1 The effect of multiple frequencies

We now study the effect of a source generating a superposition of (pseudo) sinusoidal waves at  $n_f = 4$  frequencies  $f_1^* = 400$  Hz,  $f_2^* = 300$  Hz,  $f_3^* = 200$  Hz, and  $f_4^* = 100$  Hz. Our goal is to study non-linear effects and their consequences on the sweet spot found for each frequency separately, and that found by solving the problem for a multi-frequency source. A uniform discretization of 9660 points was used for  $\Omega$ . Contiguous points are at a distance of 0.04 m, achieving more than 19 points per wavelength in the worst case. The results are shown in the Fig. 10. Observe the sweet spots generated over  $\Omega$  cover 54.3% of  $\Omega$  for 400 Hz, 73.3% for 300 Hz, 85.5% for 200 Hz and 91% for 100 Hz. The sweet spot for the multi-frequency source covered 52% of  $\Omega$ . In our standard setup it is easier to generate larger sweet spots at low frequencies, and these decrease as the frequency of the source increases. Furthermore, the sweet spots seem to be roughly nested as the frequency increases. Interestingly, the sweet spot generated for the multi-frequency source is comparable to that obtained at the highest frequency. This suggests that, in general, the sweet spot generated by our method for a multi-frequency source will be dominated by the frequency that is harder to approximate. This also yields insight into the setups for which a large sweet spot may be generated for a multi-frequency source.

### 6.2.2 Multiple zone control

The problem of creating a sound scene in a zone while keeping another silent has been extensively studied in the spatial sound literature, e.g. [55, 56]. Here we show our methods provide a solution to this problem. We consider the instance shown in Fig. 4c where  $u_0$  is equal to 0 over the silent zone as shown in Fig. 11. In the silent zone we fix a psycho-acoustic tolerance of 20 dB above the absolute threshold of hearing, whereas in the zone for the sound scene, i.e., the sound zone, we keep the van de Par model as before.

Since the silence zone is 24 times smaller than the sound zone, we balance the problem by choosing a non-uniform measure  $\mu$  that takes the value 24 over the silent zone and 1 over the sound zone. A uniform discretization of 3274 points was used for the sound zone and 332 for the silence zone. Contiguous points are at a maximum distance of 0.075 m, achieving more than 13 points per wavelength. The results are shown in Figs. 12. Our method generates a sweet spot covering 32% of the sound zone, and 97.5% of the silent zone. Also, Fig. 12c shows that the direction of the source is correctly reproduced inside the sweet spot in the sound zone. Inside the silent zone the IDE is not incorrect but undefined. This indicates that the localization properties of the auditory scene may be correctly reproduced as well. In contrast, weighted  $L^2$ -PMM performs poorly in this *global* multi-zone instance for the same reasons explained in Section 6.1 (Figs. 12d-f). It generates a sweet spot covering 1.7% of the sound zone and 27% of the silent zone. This shows our method is flexible and can be used for *global* multi-zone instances.

## 7 Discussion

Our results show the SWEET-ReLU algorithm yields state-of-the-art results in standard numerical experiments. We believe the performance in these experiments is representative of what we would observe when using more complex psycho-acoustic models for the hearing threshold and the loud discomfort level. A key component of our method is the

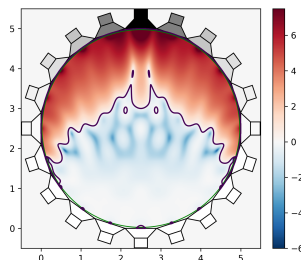


Figure 9: The effect of multiple frequencies:  $\log(1 + Tu)$  multi-frequencies.

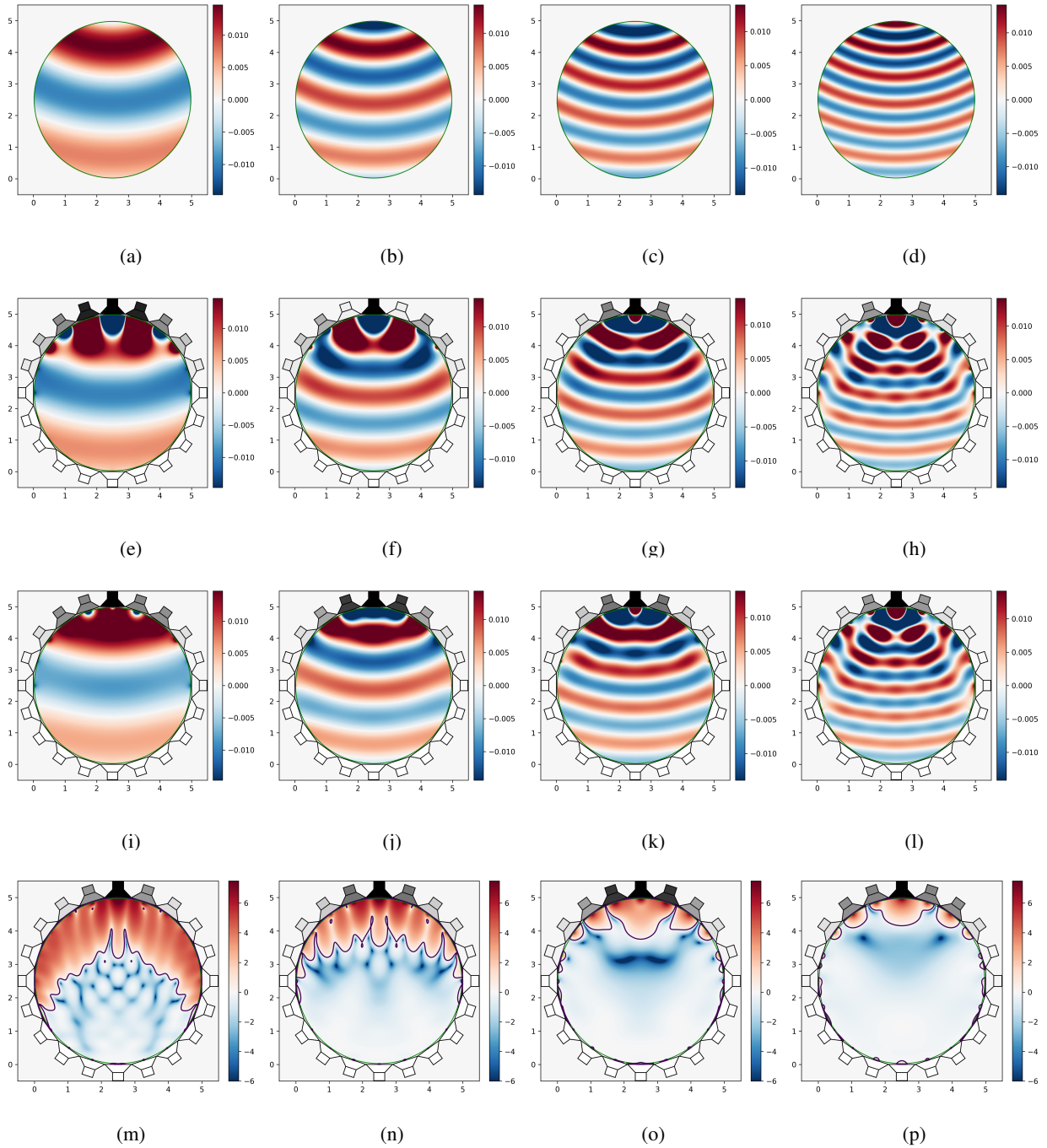


Figure 10: The effect of multiple frequencies. Rows: (i)  $u_0$ , (ii)  $u$  multi frequencies, (iii)  $u$  single frequencies, (iv)  $\log(1 + Tu)$  single frequencies. Columns: (i) 100 Hz, (ii) 200 Hz, (iii) 300 Hz, (iv) 400 Hz.

threshold map  $T$ . Although its form is quite flexible, it does not account for spatialization and other binaural effects. Extending the form of  $T$  to account for these effects is the subject of future research. However, as it is shown in [57], the overall quality of a spatial sound system can be explained to 70% by coloration or timbral fidelity, which can be characterized by monoaural effects, and 30% by spatial fidelity, which needs to be characterized by binaural effects. Furthermore, our experiments show that in some settings our method achieves a lower intensity direction error, which is a proxy for the localization error, than state-of-the-art methods. Hence, it correctly simulates the spatial properties of the auditory scene, even though we are not explicitly enforcing it.

Although we have presented numerical results modeling the loudspeakers and the virtual sources as isotropic pseudo-sinusoidal monopoles, we believe our method can be readily implemented in real settings with non-trivial sound sources. For instance, reverberation, different radiation patterns for the loudspeakers, and other time-invariant effects can be incorporated by modifying the Green’s functions  $G_k$ . For the representation of the sound scene, due to the fine discretization of the region of interest required, it may be also convenient to use an *object based* approach [1]. In this case, the target sound wave  $u_0$  is not measured with microphones, but instead is simulated when the location of the sources and their audio signals are known. Our method may be computationally expensive, as we need to solve a sequence of convex problems, precluding its use in real-time applications. Nevertheless, our multi-frequency experiments show the sweet spots nest as the frequency of a sinusoidal source increases. This suggests that an heuristic could be developed to improve the performance for multi-frequency sources. Furthermore, over a fixed instance, i.e. fixed room and loudspeaker arrangement, we may be able to approximate the map  $u_0 \mapsto u$  from several simulated instances of pairs  $(u_0, u)$ . Once approximated, the computational cost becomes negligible.

Finally, although we have not fully developed a theory for the convergence of SWEET-ReLU, our experiments show that it converges in practice. Further analysis will be the subject of future work.

## 8 Conclusion

In this work, we considered the sweet spot as the region where the a sound scene is psycho-acoustically close to a desired auditory scene. Furthermore, we developed a method that generates a sound scene that maximizes this sweet spot while guaranteeing no discomfort over a spatial region of interest. In this method, the sweet spot and the discomfort tolerance can be modeled within a flexible monoaural psycho-acoustic framework. We provided a theoretical analysis of the method, and an efficient algorithm, the SWEET-ReLU algorithm, for its numerical implementation. Over isotropic pseudo-sinusoidal monopole instances our method successfully generates a larger sweet spot than the most common state-of-the-art sound field reconstruction methods. We believe our method is a step towards a new paradigm for spatial sound reconstruction, bridging a gap between methods based on psycho-acoustic principles, and sound field reconstruction methods.

## A Proof of Proposition 1

We prove some auxiliary results. First, with a slight abuse of notation, we claim the map

$$K_B u(t, x) = \int K_B(t, t', x) u(t', x) dt',$$

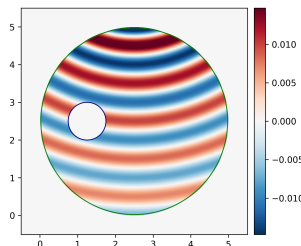


Figure 11:  $u_0$  for multiple zone setup.

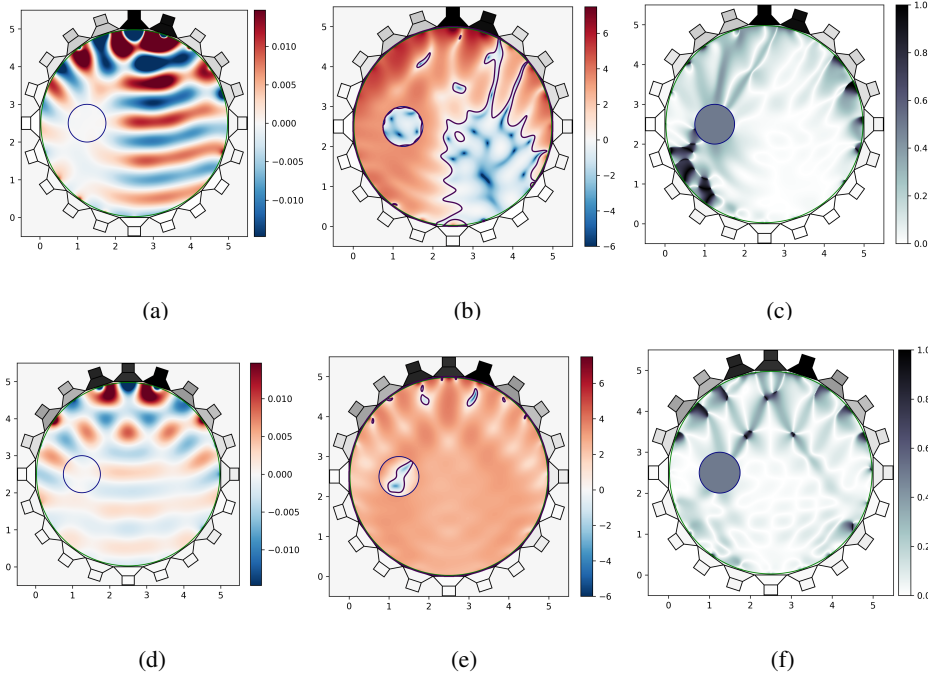


Figure 12: Multiple zone control. Rows: (i) SWEET, (ii)  $L^2$ -PMM. Columns: (i)  $u$ , (ii)  $\log(1 + Tu)$ , (iii) IDE.

where  $K_B$  satisfies the hypotheses, is continuous from  $W$  into  $W$ . To prove this, fix  $x \in \Omega$  and apply Young's inequality for integral operators [58, Theorem 0.3.1] to obtain

$$\int \left| \int K_B(t, t', x) u(t', x) dt' \right|^2 dt \leq C_B^2 \int |u(t, x)|^2 dt,$$

from where it follows that  $\|K_B u\|_W \leq C_B \|u\|_W$  and, in particular,  $K_B u \in W$ . Second, a functional  $B$  of the form (8) is bounded. This is clear from the fact that

$$|Bu(x)| = \int |K_B(u - u_0)(t, x)|^2 dt \leq C_B^2 \|u - u_0\|_W^2.$$

Third, for any  $\theta \in [0, 1]$  it is apparent that

$$B(\theta u_1 + (1 - \theta)u_2)(x) \leq \theta B(u_1)(x) + (1 - \theta)B(u_2)(x).$$

whence for almost every  $x$  the map  $u \mapsto Bu(x)$  is convex. Fourth,  $Bu$  is a measurable function by Fubini's theorem [40, Theorem 5.2.2]. Fifth,  $B$  is continuous on  $u$ . To prove this, let  $v = |K_B u_2| + |K_B u_1| + 2|K_B u_0|$  and  $w = K_B u_2 - K_B u_1$  and note that

$$|Bu_2(x) - Bu_1(x)|^2 \leq \int |v(t, x)|^2 dt \int |w(t, x)|^2 dt$$

where we used the triangle inequality, the identity  $|a^2 - b^2| = |a + b||a - b|$  and the Cauchy-Schwarz inequality. The first term is bounded, as

$$\begin{aligned} \int |v(t, x)|^2 dt &\leq 3\|K_B u_1\|_W^2 + 3\|K_B u_2\|_W^2 + 6\|K_B u_0\|_W^2 \\ &\leq 3C_B^2 (\|u_1\|_W^2 + \|u_2\|_W^2 + 2\|u_0\|_W^2), \end{aligned}$$

where we used the inequality  $(a + b + c)^2 \leq 3(a^2 + b^2 + c^2)$ . For the second, we have

$$\int |w(t, x)|^2 dt \leq \|K_B(u_1 - u_2)\|_W^2 \leq C_B^2 \|u_1 - u_2\|_W^2.$$

It follows that  $u_1 \rightarrow u_2$  in  $W$  implies  $Bu_1 \rightarrow Bu_2$  in  $L^\infty(\Omega)$  whence  $B : W \rightarrow L^\infty(\Omega)$  is continuous.

*Proof of (i):* We prove the result for  $n_b = 2$  for simplicity. Since  $\Psi$  in (9) is continuous and each  $B_k : W \rightarrow L^\infty(\Omega)$  is continuous by our auxiliary results,  $T : W \rightarrow L^\infty(\Omega)$  is continuous. Similarly, since  $\Psi$  is convex and non-decreasing on every component, for every  $\theta \in [0, 1]$  we have

$$\begin{aligned} T(\theta u_1 + (1 - \theta)u_2)(x) &\leq \Psi(\theta v_{1,1}(x) + (1 - \theta)v_{1,2}(x), \theta v_{2,1}(x) + (1 - \theta)v_{2,2}(x)) \\ &\leq \theta T u_1(x) + (1 - \theta)T u_2(x) \end{aligned}$$

where  $v_{k,j} = B_k u_j$ , proving the convexity of  $u \rightarrow Tu(x)$  for almost every  $x$ . Analogously,  $P$  is continuous and  $u \rightarrow Pu(x)$  is convex for almost every  $x$ .

*Proof of (ii):* Note that  $\Psi$  is measurable, because it is continuous, and so is  $B_k u$ . Therefore,  $T$  in (9) is measurable, and the set  $\mathcal{S}(u)$  is measurable for any  $u \in W$ .

*Proof of (iii):* We show that  $W_S$  is a family functions  $\Omega \mapsto L^2(\mathbb{R})$  that is bounded, equicontinuous, and defined on a separable metric space, whence, by Arzelà-Ascoli's theorem [59, Theorem 11.28], is compact with respect to the uniform norm, which coincides with the  $W$ -norm. Let  $\gamma_{\max}$  be the uniform bound on  $\|c_k\|_{L^2}$ . Consider the map  $\Omega \rightarrow L^2(\Omega)$  given by  $x \rightarrow u_x$  where  $u_x$  denotes the function  $t \mapsto u(t, x)$ . Since each  $G_k$  is bounded on  $I_c \times \bar{\Omega}$  then

$$\begin{aligned} \int |u(t, x)|^2 dt &\leq n_s \sum_{k=1}^{n_s} \int_{I_c} |\hat{c}_k(f)|^2 |G_k(f, x)|^2 df \\ &\leq n_s \sum_{k=1}^{n_s} \sup_{(f, x) \in I_c \times \bar{\Omega}} |G_k(f, x)|^2 \|c_k\|_{L^2}^2 \end{aligned}$$

whence  $x \mapsto u_x$  is uniformly bounded. To prove equicontinuity, fix  $\varepsilon > 0$ . Since each  $G_k$  is continuous on the compact set  $I_c \times \bar{\Omega}$ , we can find  $\delta > 0$  such that for any  $|x - y| < \delta$  and  $f \in I_c$  we have  $|G_k(f, x) - G_k(f, y)| < \varepsilon/n_s^2 \gamma_{\max}^2$ . Then

$$\int |u(t, x) - u(t, y)|^2 dt \leq n_s \sum_{k=1}^{n_s} \int_{I_c} |\hat{c}_k(f)|^2 |G_k(f, y) - G_k(f, x)|^2 df < n_s \gamma_{\max}^2 \left( n_s \frac{\varepsilon}{n_s^2 \gamma_{\max}^2} \right) = \varepsilon$$

showing not only that  $x \mapsto u_x$  is continuous, but equicontinuous. We conclude  $W_S$  is compact in  $W$ .

*Proof of (iv):* We omit details for brevity. The map  $P : W \rightarrow L^\infty(\Omega)$  is continuous by the same arguments we used in the proof of (i). Then, since non-strict inequalities are preserved under limits,  $\mathcal{P}$  is closed.

## B Proof of Proposition 8

Let  $u \in W_S$ , and let  $v := u - u_0$ . Define the auxiliary function

$$h(t, x) = \left| \int K_B(t, t', x) v(t', x) dt' \right|.$$

Then,

$$|Bu(x) - Bu(y)|^2 \leq \left( \int (h(t, x) + h(t, y))^2 dt \right) \left( \int (h(t, x) - h(t, y))^2 dt \right)$$

where we used the identity  $|a^2 - b^2| = |a + b||a - b|$  and the Cauchy-Schwarz inequality. For the first term, by a similar argument as that in the proof of Proposition 1 we deduce

$$\int (h(t, x) + h(t, y))^2 dt \leq 2 \int h(t, x)^2 dt + 2 \int h(t, y)^2 dt \leq 4C_B^2 \|v\|_W^2$$

whence it is bounded. For the second term, note first that

$$|h(t, x) - h(t, y)| \leq \left| \int K_B(t, t', x) (v(t', x) - v(t', y)) dt' \right| + \left| \int (K_B(t, t', x) - K_B(t, t', y)) v(t', y) dt' \right|.$$

By hypothesis, the first integral can be bounded as

$$\left| \int K_B(t, t', x) (v(t', x) - v(t', y)) dt' \right|^2 \leq \left( \int f_K(t, t') |v(t', x) - v(t', y)| dt' \right)^2$$

$$\leq \left( \int f_K(t, t')^2 dt' \right) \left( \int |v(t', x) - v(t', y)|^2 dt' \right)$$

whereas the second can be bounded as

$$\left| \int (K_B(t, t', x) - K_B(t, t', y))v(t', y)dt' \right|^2 \leq \left( \int |K_B(t, t', x) - K_B(t, t', y)|^2 dt' \right) \left( \int |v(t', y)|^2 dt' \right)$$

Then

$$\begin{aligned} \int (h(t, x) - h(t, y))^2 dt &\leq 2 \int \left| \int K_B(t, t', x)(v(t', x) - v(t', y))dt' \right|^2 dt \\ &\quad + 2 \int \left| \int (K_B(t, t', x) - K_B(t, t', y))v(t', y)dt' \right|^2 dt \\ &\leq 2 \left( \int \int f_K(t, t') dt dt' \right) \int |v(t', x) - v(t', y)|^2 dt' \\ &\quad + 2\|v\|_W^2 \int \int |K_B(t, t', x) - K_B(t, t', y)|^2 dt' dt. \end{aligned}$$

Therefore, it suffices to show the integrals on the right-hand side tend to zero as  $x - y$  tends to zero. For the first term we have

$$\int |v(t', x) - v(t', y)|^2 dt' = \int |u(t', x) - u(t', y)|^2 dt'.$$

By the proof of (iii) in Proposition 1 we know  $u \in W_S$  implies  $x \rightarrow u(\cdot, x)$  is a continuous map  $\Omega \mapsto L^2(\mathbb{R})$ . Hence, the above tends to zero as  $x - y \rightarrow 0$ . For the second term, we have the bound

$$|K_B(t, t', x) - K_B(t, t', y)|^2 \leq 2f_K(t, t')^2$$

whence the integrand is dominated and by Lebesgue's dominated convergence theorem we deduce that

$$\int \int |K_B(t, t', x) - K_B(t, t', y)|^2 dt' dt \rightarrow 0$$

as  $x - y \rightarrow 0$ . Hence,

$$\int (h(t, x) - h(t, y))^2 dt \rightarrow 0$$

as  $x - y \rightarrow 0$  and  $x \rightarrow h(\cdot, x)$  is a continuous map  $\Omega \mapsto L^2(\mathbb{R})$ .

## Acknowledgment

C. A. SL. was partially funded by ANID – FONDECYT – 1211643, ANID – Millennium Science Initiative Program – NCN17\_059 and ANID – Millennium Science Initiative Program – NCN17\_129.

## References

- [1] Sascha Spors, Hagen Wierstorf, Alexander Raake, Frank Melchior, Matthias Frank, and Franz Zotter. Spatial sound with loudspeakers and its perception: A review of the current state. *Proceedings of the IEEE*, 101(9):1920–1938, 2013.
- [2] Jens Blauert. *Spatial hearing: the psychophysics of human sound localization*. MIT press, 1997.
- [3] Filippo M Fazi and Philip A Nelson. The ill-conditioning problem in sound field reconstruction. In *Audio Engineering Society Convention 123*. Audio Engineering Society, 2007.
- [4] Filippo M Fazi and Philip A Nelson. Nonuniqueness of the solution of the sound field reproduction problem with boundary pressure control. *Acta Acustica united with Acustica*, 98(1):1–14, 2012.
- [5] Jérôme Daniel. *Représentation de champs acoustiques, application à la transmission et à la reproduction de scènes sonores complexes dans un contexte multimédia*. PhD thesis, University of Paris VI, 2000.
- [6] Michael A Gerzon. Periphony: With-height sound reproduction. *Journal of the audio engineering society*, 21(1):2–10, 1973.

- 
- [7] Jérôme Daniel, Sebastien Moreau, and Rozenn Nicol. Further investigations of high-order ambisonics and wavefield synthesis for holophonic sound imaging. In *Audio Engineering Society Convention 114*. Audio Engineering Society, 2003.
- [8] Darren B Ward and Thushara D Abhayapala. Reproduction of a plane-wave sound field using an array of loudspeakers. *IEEE/ACM Transactions on Audio Speech and Language Processing*, 9, 2001.
- [9] Ole Kirkeby and Philip A Nelson. Reproduction of plane wave sound fields. *The Journal of the Acoustical Society of America*, 94(5):2992–3000, 1993.
- [10] Georgios N. Lilis, Daniele Angelosante, and Georgios B. Giannakis. Sound field reproduction using the lasso. *IEEE Transactions on Audio, Speech and Language Processing*, 18:1902–1912, 2010.
- [11] Edwin Verheijen. *Sound Reproduction by Wave Field Synthesis*. PhD thesis, Delft University of Technology, 1997.
- [12] Augustinus J Berkhout, Diemer de Vries, and Peter Vogel. Acoustic control by wave field synthesis. *The Journal of the Acoustical Society of America*, 93(5):2764–2778, 1993.
- [13] Diemer de Vries and Chen Xiaoping. Aes monograph: Wave field synthesis (continued). *Audio Engineering*, page 5, 2014.
- [14] Sascha Spors, Rudolf Rabenstein, and Jens Ahrens. The theory of wave field synthesis revisited. In *In 124th Convention of the AES*. Citeseer, 2008.
- [15] Hagen Wierstorf, Alexander Raake, and Sascha Spors. Localization in wave field synthesis and higher order ambisonics at different positions within the listening area. In *Proceeding of German Annual Conference on Acoustics (DAGA)*, 2013.
- [16] Hagen Wierstorf, Christoph Hohnerlein, Sascha Spors, and Alexander Raake. Coloration in wave field synthesis. In *Audio Engineering Society Conference: 55th International Conference: Spatial Audio*. Audio Engineering Society, 2014.
- [17] Sascha Spors and Jens Ahrens. A comparison of wave field synthesis and higher-order ambisonics with respect to physical properties and spatial sampling. In *Audio Engineering Society Convention 125*. Audio Engineering Society, 2008.
- [18] Filippo M Fazi, Philip A Nelson, and Roland Potthast. Analogies and differences between three methods for sound field reproduction. *Relation*, 10:3, 2009.
- [19] Filippo Maria Fazi and Philip A. Nelson. A theoretical study of sound field reconstruction techniques. In *19th International Congress on Acoustics*, September 2007.
- [20] Eberhard Zwicker and Hugo Fastl. *Psychoacoustics: Facts and models*, volume 22. Springer Science & Business Media, 2007.
- [21] James D Johnston and Yin Hay Vicky Lam. Perceptual soundfield reconstruction. In *Audio Engineering Society Convention 109*. Audio Engineering Society, 2000.
- [22] Enzo De Sena, Huseyin Hacihabiboglu, and Zoran Cvetkovic. Analysis and design of multichannel systems for perceptual sound field reconstruction. *IEEE Transactions on Audio, Speech and Language Processing*, 21:1653–1665, 2013.
- [23] Tim Ziemer and Rolf Bader. Psychoacoustic sound field synthesis for musical instrument radiation characteristics. *AES: Journal of the Audio Engineering Society*, 65:482–496, 6 2017.
- [24] Taewoong Lee, Jesper Kjaer Nielsen, and Mads Graesboll Christensen. Signal-adaptive and perceptually optimized sound zones with variable span trade-off filters. *IEEE/ACM Transactions on Audio Speech and Language Processing*, 28:2412–2426, 2020.
- [25] Steven van de Par, Armin Kohlrausch, Richard Heusdens, Jesper Jensen, and Søren Holdt Jensen. A perceptual model for sinusoidal audio coding based on spectral integration. *EURASIP Journal on Advances in Signal Processing*, 2005(9):1–13, 2005.
- [26] Lawrence C. Evans. *Partial Differential Equations*. American Mathematical Society, 2nd edition, 2010.
- [27] Philippe-Aubert Gauthier, Alain Berry, and Wieslaw Woszczyk. Sound-field reproduction in-room using optimal control techniques: Simulations in the frequency domain. *The Journal of the Acoustical Society of America*, 117:662–678, 2 2005.
- [28] Terence Betlehem and Thushara D Abhayapala. Theory and design of sound field reproduction in reverberant rooms. *The Journal of the Acoustical Society of America*, 117(4):2100–2111, 2005.

- 
- [29] Earl G Williams. *Fourier acoustics: sound radiation and nearfield acoustical holography*. Academic press, 1999.
- [30] Steven G. Krantz and Harold R. Parks. *A Primer of Real Analytic Functions*. Birkhäuser Boston, Boston, MA, 2002.
- [31] Morten L. Jepsen, Stephan D. Ewert, and Torsten Dau. A computational model of human auditory signal processing and perception. *The Journal of the Acoustical Society of America*, 124:422–438, 7 2008.
- [32] Sascha Disch, Steven van de Par, Andreas Niedermeier, Elena Burdiel Pérez, Ane Berasategui Ceberio, and Bernd Edler. Improved psychoacoustic model for efficient perceptual audio codecs. In *Audio Engineering Society Convention 145*. Audio Engineering Society, 2018.
- [33] Jan H. Plasberg and W. Bastiaan Kleijn. The sensitivity matrix: Using advanced auditory models in speech and audio processing. *IEEE Transactions on Audio, Speech and Language Processing*, 15:310–319, 1 2007.
- [34] Cees H. Taal, Richard C. Hendriks, and Richard Heusdens. A low-complexity spectro-temporal distortion measure for audio processing applications. *IEEE Transactions on Audio, Speech and Language Processing*, 20:1553–1564, 2012.
- [35] Ted Painter and Andreas Spanias. Perceptual coding of digital audio. *Proceedings of the IEEE*, 88(4):451–515, 2000.
- [36] Marina Bosi and Richard E Goldberg. *Introduction to digital audio coding and standards*, volume 721. Springer Science & Business Media, 2012.
- [37] Keila Alessandra Baraldi Knobel and Tanit Ganz Sanchez. Nível de desconforto para sensação de intensidade em indivíduos com audição normal. *Pró-Fono Revista de Atualização Científica*, 18(1):31–40, 2006.
- [38] LaGuinn P Sherlock and Craig Formby. Estimates of loudness, loudness discomfort, and the auditory dynamic range: normative estimates, comparison of procedures, and test-retest reliability. *Journal of the American Academy of Audiology*, 16(02):085–100, 2005.
- [39] A. Benedek and R. Panzone. The space LP, with mixed norm. *Duke Mathematical Journal*, 28(3):301–324, sep 1961.
- [40] Donald L. Cohn. *Measure Theory*. Birkhäuser Advanced Texts Basler Lehrbücher. Springer New York, New York, NY, 2nd edition, 2013.
- [41] Halsey Lawrence Royden and Patrick Fitzpatrick. *Real analysis*. Pearson, 4th edition, 2010.
- [42] Heinz H. Bauschke and Patrick L. Combettes. *Convex Analysis and Monotone Operator Theory in Hilbert Spaces*. CMS Books in Mathematics. Springer New York, New York, NY, 2011.
- [43] Pham Dinh Tao and Le Thi Hoai An. Convex Analysis Approach to D.C. Programming: Theory, Algorithms and Applications. *Acta Mathematica Vietnamica*, 22(1):289–355, 1997.
- [44] R. Horst and N. V. Thoai. DC Programming: Overview. *Journal of Optimization Theory and Applications*, 103(1):1–43, oct 1999.
- [45] Thomas Lipp and Stephen Boyd. Variations and extension of the convex–concave procedure. *Optimization and Engineering*, 17(2):263–287, jun 2016.
- [46] Viorel Barbu and Teodor Precupanu. *Convexity and Optimization in Banach Spaces*. Springer Monographs in Mathematics. Springer Netherlands, Dordrecht, 4th edition, 2012.
- [47] Jean-Pierre Aubin and Hélène Frankowska. *Set-Valued Analysis*. Birkhauser, 1990.
- [48] Ernst Terhardt. Calculating virtual pitch. *Hearing research*, 1(2):155–182, 1979.
- [49] Brian R Glasberg and Brian CJ Moore. Derivation of auditory filter shapes from notched-noise data. *Hearing research*, 47(1-2):103–138, 1990.
- [50] Alfio Quarteroni, Riccardo Sacco, and Fausto Saleri. *Numerical mathematics*, volume 37. Springer Science & Business Media, 2010.
- [51] Steven Diamond and Stephen Boyd. CVXPY: A Python-embedded modeling language for convex optimization. *Journal of Machine Learning Research*, 17(83):1–5, 2016.
- [52] Akshay Agrawal, Robin Verschueren, Steven Diamond, and Stephen Boyd. A rewriting system for convex optimization problems. *Journal of Control and Decision*, 5(1):42–60, 2018.
- [53] MOSEK ApS. *The MOSEK optimization toolbox for Python manual. Version 9.2.44*, 2019.
- [54] Hagen Wierstorf and Sascha Spors. Sound field synthesis toolbox. In *Audio Engineering Society Convention 132*. Audio Engineering Society, 2012.

- 
- [55] Mark Poletti. An investigation of 2-d multizone surround sound systems. In *Audio Engineering Society Convention 125*. Audio Engineering Society, 2008.
- [56] Yan Jennifer Wu and Thushara D Abhayapala. Spatial multizone soundfield reproduction: Theory and design. *IEEE Transactions on audio, speech, and language processing*, 19(6):1711–1720, 2010.
- [57] Francis Rumsey, Sławomir Zieliński, Rafael Kassier, and Søren Bech. On the relative importance of spatial and timbral fidelities in judgments of degraded multichannel audio quality. *The Journal of the Acoustical Society of America*, 118(2):968–976, 2005.
- [58] Christopher D. Sogge. *Fourier Integrals in Classical Analysis*. Cambridge University Press, Cambridge, 2nd edition, 2017.
- [59] Walter Rudin. *Real and Complex Analysis*. McGraw-Hill Education, 3rd edition, 1986.